POZNAŃ UNIVERSITY OF LIFE SCIENCES
FACULTY OF ENVIRONMENTAL ENGINEERING AND MECHANICAL ENGINEERING
DEPARTMENT OF ECOLOGY AND ENVIRONMENTAL PROTECTION
LABORATORY OF BIOCLIMATOLOGY

AUTOREFERAT

PhD dissertation

Application of ground, airborne and satellite remote sensing techniques to assess the Sun-induced fluorescence and reflectance of different ecosystems

Subhajit Bandopadhyay

Poznań, November 2021

Thesis committee

Thesis supervisor

Prof. dr hab. Radosław Juszczak
Professor and Head of Laboratory of Bioclimatology
Department of Ecology and Environmental Protection
Faculty of Environmental and Mechanical Engineering
Poznań University of Life Sciences
Piątkowska 94
60-649 Poznań, Poland

Thesis co-supervisor

Prof. UPP dr. hab. Anshu Rastogi
Department of Ecology and Environmental Protection
Faculty of Environmental and Mechanical Engineering
Poznań University of Life Sciences
Piątkowska 94
60-649 Poznań, Poland

Guest Scientist at University of Twente,
Faculty of Geo-Information Science and Earth Observation (ITC)
Enschede, The Netherlands

Committee Members

Prof. dr hab. Klaudia Borowiak	Poznań University of Life Sciences, Poland
Prof. dr hab. Jolanta Komisarek	Poznań University of Life Sciences, Poland
Prof. dr hab. Bogdan H. Chojnicki	Poznań University of Life Sciences, Poland
Prof. dr hab. Mariusz Sojka	Poznań University of Life Sciences, Poland

Bandopadhyay, S.
Application of ground, airborne and satellite remote sensing techniques to assess the Sun-induced fluorescence (SIF) and reflectance (R) of different ecosystems Pages: 231
PhD thesis, Poznań University of Life Sciences, Poznań, Poland

Acknowledgments

I would love to take this opportunity to present my honest gratitude to my parents for their sacrifices and valuable support to make my doctorate possible. They always supported me at every point of my life, which may not express in words. They boosted me with their moral support and valuable suggestions to keep my energy and confidence to tackle every hurdle. Their love, care, and support never let me feel alone and far from home. I am fortunate to have such parents. I want to thank my wife (Maitri) for her love and dedicated support to continue my work. She is always beside me in every decision of my life and encourages me to efficiently finish my doctorate.

I want to express my sincere gratitude to my Ph.D. supervisor Prof. dr hab. Radosław Juszczak, for his continuous support, efficient supervisory, and motivation to complete my Ph.D. successfully. I would also extend my sincere guidance to my co-supervisor Prof. UPP dr. hab. Anshu Rastogi for his support in difficult times and guidance that immensely helped me to achieve the desired objectives. My Ph.D. would not have been possible without their friendly nature, dedicated time, inspiration, and support. I would also like to thank my thesis committee members, Prof. dr hab. Klaudia Borowiak, Prof. UPP dr hab. Bogdan H. Chojnicki, Prof. dr hab. Mariusz Sojka, for their encouragement and guidance. I am also very thankful to Prof. Uwe Rascher from IBG-2: Plant Sciences, Forschungszentrum Jülich, Germany and dr. Sergio Cogliati from Department of Earth and Environmental Sciences, University of Milano-Bicocca, Italy for their support, supervision and as a valuable co-authors of the publications. I would also like to thank dr. Bringfried Pflug from Institute for Remote Sensing, German Aerospace Center (DLR), Berlin, Germany for his support and guidance during my STSM visit at DLR, Berlin. I would also extend my sincere gratitude and thanks to dr. Andreas Hueni from Remote Sensing Laboratories (RSL), Department of Geography, University of Zurich, Switzerland for his intense support and guidance during the NAWA Iwanowska Programme.

I would also like to thank my super-cool lab mates, Dr. Marcin Stróżecki, Michal Antala, Kamila Harenda, Patryk Poczta, Mateusz Samson, Damian Józefczyk, and other office staff members from Laboratory of Bioclimatology, Poznan University of Life Sciences. I would also like to thank my RSL colleagues, Daria, Carmen for their support during my stay at RSL, University of Zurich. Furthermore, I would also like to thank the COST Action "*Optical synergies for spatiotemporal SENsing of Scalable ECOphysiological traits*" (SENSECO) community and particularly the young SENSECO community for collaboration and networking activities during my PhD studies.

I would also like to thank Prof. Chandana Mitra, from Auburn University, Dr. Shovan Lal Chattoraj from ISRO, Dr. Krishnendu Gupta from Visva-Bharati for their support and guidance for PhD studies. I am happy to express my thanks to Dany Alexander, Subhasis Ghosh, Ujjal Gorai, Rahul Deb Das, Lopita Pal for their

supports. I also want to thank my brothers Deep, Surajit, Abhishek, and my extended family members.
I am fortunate to have the grace of God because none of these would have been possible without their mercy. Finally, I am thankful to everyone who provided valuable support, encouragement, and motivation to succeed in my research.

Table of contents

List of published papers constituting the basis of the PhD dissertation

Publication 1

Subhajit Bandopadhyay, Anshu Rastogi, and Radosław Juszczak (**2020**) "Review of Top-of-Canopy Sun-Induced Fluorescence (SIF) studies from ground, UAV, airborne to spaceborne observations." *Sensors*, 20, 1144. DOI: https://doi.org/10.3390/s20041144 **(IF 3.576)**

Publication 2

Subhajit Bandopadhyay, Anshu Rastogi, Uwe Rascher, Patrick Rademske, Anke Schickling, Sergio Cogliati, Tommaso Julitta, Alasdair Mac Arthur, Andreas Hueni, Enrico Tomelleri, Marco Celesti, Andreas Burkart, Marcin Stróżecki, Karolina Sakowska, Maciej Gąka, Stanisław Rosadziński, Mariusz Sojka, Maria-Daniel Iordache, Ils Reusen, Christiaan Van Der Tol, Alexander Damm, Dirk Schuettemeyer, Radosław Juszczak (**2019**) "Hyplant-derived sun-induced fluorescence—A new opportunity to disentangle complex vegetation signals from diverse vegetation types." *Remote Sensing*, 11, (14), 1691. DOI: https://doi.org/10.3390/rs11141691 **(IF 4.848)**

Publication 3

Subhajit Bandopadhyay, Anshu Rastogi, Sergio Cogliati, Uwe Rascher, Maciej Gąbka, and Radosław Juszczak (**2021**) "Can Vegetation Indices Serve as Proxies for Potential Sun-Induced Fluorescence (SIF)? A Fuzzy Simulation Approach on Airborne Imaging Spectroscopy Data." *Remote Sensing*, 13, no. 13, 2545. DOI: https://doi.org/10.3390/rs13132545 **(IF 4.848)**

Publication 4

Subhajit Bandopadhyay, Lopita Pal, and Rahul Deb Das (**2021**) "Predicting gross primary productivity and PsnNet over a mixed ecosystem under tropical seasonal variability: a comparative study between different machine learning models and correlation-based statistical approaches." *Journal of Applied Remote Sensing*, 15, 1, 014523. DOI: https://doi.org/10.1117/1.JRS.15.014523 **(IF 1.53)**

PhD's Author contribution to the publications

Subhajit Bandopadhyay is the author of this PhD thesis submitted towards the fulfilment of the PhD degree at Poznań University of the Life Sciences, Poznań, Poland. He is the 'lead primary author' of all four publications and has done majority of the research independently and wrote manuscripts under the supervision of his supervisors.

Publication 1: Subhajit Bandopadhyay was responsible for (i) the collection of all SIF related studies incorporating ground, airborne, UAV and spaceborne sensors and developed the database, (ii) conceptualized and design the study, (iii) prepared the tables and figures, (iv) wrote, reviewed, edited, and corrected the full manuscript and submit.

Contribution: 80%

Publication 2: Subhajit Bandopadhyay has performed (i) collection of the raw airborne datasets from 2015 SWAMP airborne campaign, (ii) process the data and perform the analysis including calibration and validation of the maps (i.e. airborne and ground datasets), (iii) developed maps, figures and tables, (iv) design and conceptualized the manuscript, (v) formulate the processing chain and methodology, (vi) wrote, reviewed, edited, and corrected the full manuscript and submit.

Contribution: 45%

Publication 3: Subhajit Bandopadhyay developed the SIF_{fuzzy} and $SIF_{fuzzy\text{-}APAR}$ model. Along with he was responsible for (i) collection of the datasets, (ii) develop the fuzzy model, (iii) optimize the model, (iv) conceptualized and design the research, (v) created the processing chain and process the data, (vi) developed maps, figures and tables, (vii) wrote, reviewed, edited, and corrected the full manuscript and submit.

Contribution: 65%

Publication 4: Subhajit Bandopadhyay was responsible for (i) collection of the spaceborne data (i.e. Landsat 8 OLI and MODIS), (ii) developed the method of research, (iii) process the data (i.e. atmospheric correction, downscaling of the data), (iv) design sample collection framework, (v) collected the sample and processing of data through correlation models and machine learning models, (v) conceptualized and design the manuscript, (vi) developed maps, figures and tables, (vii) wrote, reviewed, edited, and corrected the full manuscript and submit.

Contribution: 65%

Summary

Sun-induced fluorescence (SIF) has been emerged as unique and relatively novel remote sensing (RS) signal in the contemporary era to understand and monitor the terrestrial vegetation activity as well as their structural and functional diversity. The research and applicability potential of SIF has been well recognized by scientists. The SIF signal is emitted from the core of photosynthetic processes and is directly linked to plant photosynthetic activity and plant health conditions. As SIF signal originates from the core of photosynthetic activity, which is an important biochemical process in terrestrial ecosystems that regulates gas exchange between the atmosphere and biosphere, the significance of SIF science is high and is permanently increasing with development of new methods of its retrieval from spectroscopic data and application of new remote sensing platforms and systems to measure SIF from ground, near-atmosphere (UAV, airborne) and space (satellites). The advancement of optical and hyperspectral RS technologies offers currently unique possibilities to capture and estimate SIF signals and reflectances (R) in order to monitor the status of terrestrial vegetation, their phenology, and ecosystem functions. Narrow-band hyperspectral imaging spectrometers are rapidly evolving and provide unique opportunities for monitoring SIF signals at both O_2 absorption bands and R at different wavelengths.

In this PhD research, HyPlant airborne imaging spectrometer (the airborne demonstrator of European Space Agency's FLEX FLORIS satellite) has been extensively implemented to estimate, monitor, and model SIF signals at both O_2 absorption bands over heterogeneous peatland and surrounded forest and grasslands ecosystems for the first time. HyPlant is a high-performance airborne spectrometer to measure R and SIF developed by Forschungszentrum Jülich, (Germany) in cooperation with SPECIM Spectral Imaging Ltd. (Finland). Most important part of the research conducted within this PhD is based on the HyPlant airborne campaign held in July 2015 over Rzecin peatland located in the western part of Poland.

The PhD is based on the four research papers published in period 2019-2021 in journals with impact factor from 1.53 to 4.85. The structure of the PhD reflects the content of these papers, starts from general introduction to the PhD topic and its objectives and applied methods and ends with summary and conclusions. This PhD thesis is divided into six chapters.

Chapter 1 outlines a general introduction to the PhD dissertation and SIF. The objectives and hypothesis of the thesis have been discussed in this chapter. The origin and types of the SIF signals from plant photosynthetic activity has been also discussed. The HyPlant airborne campaign details along with the short description of the applied methods used to verify the research hypothesis have been also described.

Chapter 2 addresses the comprehensive and current state-of-the-art review on Top-of-Canopy (TOC) SIF studies from the ground, UAV, airborne to spaceborne observations. The review focuses on the studies that have been conducted on SIF

measurement techniques, retrieval algorithms, modelling, application and validation, incorporating different RS observations platforms and sensor along with their present limitations.

Chapter 3 represents the first airborne SIF maps at both O_2 absorption bands at 687nm and 760nm of the Rzecin peatland and surrounding ecosystems. This chapter also shows the degree of agreement between SIF signals at both O_2 absorption bands and spectral indices which were associated with plant structural and functional traits. It also represents the sensitivity of the SIF signals with productivity gradient at ecosystem scale and plant community scale.

Chapter 4 is a machine-learning-based methodological model chapter that shows the simulation of SIF signals at 687nm and 760nm in a step-wise approximation manner from simple spectral vegetation indices (NDVI, SR, NDVIre, EVI, PRI) using airborne imaging spectrometric data through fuzzy modelling and data integration techniques. It was shown that the fuzzy modelled approach can accurately approximate the SIF signals at both O_2 absorption bands from vegetation traits as well as can capture the structural and functional diversity of the vegetation at the ecosystem scale.

Chapter 5 represents the importance of reflectance satellite-based vegetation spectroscopic measurements through various spectral indices, in estimations of gross primary productivity (GPP) and net photosynthesis (PsnNet) of tropical ecosystems. It outlines a comparative investigation of different correlation methods (i.e., Pearson product, Spearman rank, and Kendall rank) and supervised machine learning models (i.e., random forest, conditional inference forests, and quantile regression forests) to explore the agreement and possibility of prediction of GPP and PsnNet based on spectral indices, tasselled cap transformations, and reflectances over a mixed ecosystems under tropical seasonal variability.

Chapter 6 provides the synthesis and conclusions of the PhD thesis. The overall conclusion indicates that the developing science about SIF incorporating modern RS technology has emerged and opened new direction advancing the knowledge in terrestrial vegetation and the global carbon cycle, with the development of the ground-based instruments such as FloXbox (JB Hyperspectral Devices GmbH, Germany) and PICCOLO-DOPPIO (The University of Edinburgh, UK), airborne sensors like HyPlant, and upcoming space missions like the Fluorescence Explorer (FLEX) Fluorescence Imaging Spectrometer (FLORIS) of European Space Agency (ESA) satellite, etc.

The PhD results provided the first experimental evidence that through the red (SIF_{687}) and far-red (SIF_{760}) chlorophyll fluorescence signals it is possible to capture the huge spatial heterogeneity of peatland, forest and grassland ecosystems representing different photosynthetic activity, biochemical and structural traits of diversified plant communities and hence to facilitate the assessments of the wide functional diversity of vegetation canopies. Furthermore, it has been observed that the developed fuzzy modelling techniques named SIFfuzzy and SIFfuzzy-APAR can approximate the original SIF signals at both O_2 absorption bands with high accuracy and also is able to represent the structural and functional diversity of plant canopies.

This research has also indicated that the differences in meteorological and environmental conditions have an impact on plant functional activities observed through satellite observed reflectances that significantly differ the prediction process of GPP and PsnNet based on the remote sensing approaches.

Keywords: Sun-induced fluorescence (SIF); Spectral vegetation indices; *HyPlant*; Imaging spectroscopy; Fuzzy modelling; Machine learning; Gross primary productivity (GPP); Peatland; Forest; Grassland.

Streszczenie

Fluorescencja indukowana promieniowaniem słonecznym (SIF) jest unikalnym i stosunkowo nowym sygnałem teledetekcyjnym (RS) wykorzystywanym do zrozumienia i monitorowania aktywności roślinności ekosystemów lądowych, a także różnorodności strukturalnej i funkcjonalnej naturalnych ekosystemów. Potencjał badawczy i aplikacyjny SIF jest dobrze rozpoznany przez naukowców. SIF jest sygnałem emitowanym przez cząsteczki chlorofilu i jest bezpośrednio powiązany z aktywnością fotosyntetyczną roślin oraz ich warunkami zdrowotnymi. Ponieważ SIF jest powiązany z aktywnością fotosyntetyczną roślin, która jest ważnym procesem biochemicznym w ekosystemach lądowych regulującym wymianę gazową między atmosferą a biosferą, znaczenie nauki o SIF jest bardzo duże i ciągle rośnie wraz z wprowadzaniem nowych metod szacowania SIF na podstawie danych spektrometrycznych oraz stosowanie nowych platform teledetekcyjnych i systemów do pomiarów SIF z poziomu gruntu, z poziomu lotniczego i z przestrzeni kosmicznej (za pomocą satelitów). Postęp w optycznych i hiperspektralnych technologiach teledetekcyjnych oferuje obecnie unikalne możliwości pomiaru i szacowania SIF oraz reflektancji (R) w celu monitorowania stanu roślinności ekosystemów lądowych, ich fenologii i funkcji ekosystemowych. Wąskopasmowe spektrometry do obrazowania hiperspektralnego szybko ewoluują i zapewniają wyjątkowe możliwości monitorowania sygnałów SIF w obu pasmach absorpcji O_2 i reflektancji przy różnych długościach fal.
W ramach badań stanowiących podstawę niniejszej rozprawy doktorskiej wykorzystany został spektrometr HyPlant do obrazowania hiperspektralnego z poziomu lotniczego (prototypowy demonstrator satelity FLEX FLORIS Europejskiej Agencji Kosmicznej). System ten po raz pierwszy wykorzystano do szacowania, monitorowania i modelowania sygnałów SIF w obu pasmach absorpcji O_2 dla niejednorodnych powierzchni torfowiska oraz przyległych ekosystemów leśnych i łąkowych. HyPlant to wysokowydajny spektrometr do pomiaru R i SIF z poziomu lotniczego opracowany przez Forschungszentrum Jülich (Niemcy) we współpracy ze SPECIM Spectral Imaging Ltd. (Finlandia). Najważniejsza część badań wykonanych w ramach niniejszej rozprawy doktorskiej opiera się na wynikach

nalotów z kampanii lotniczej z systemem HyPlant z lipca 2015 r. wykonanych nad torfowiskiem Rzecińskm zlokalizowanym w zachodniej części Polski.
Niniejsza rozprawa doktorska opiera się na cyklu czterech artykułów naukowych opublikowanych w latach 2019-2021 w czasopismach o współczynniku wpływu od 1,53 do 4,85. Struktura doktoratu odzwierciedla treść tych artykułów, zaczyna się od ogólnego wprowadzenia do tematu doktoratu, zakładanych celów oraz stosowanych metod, a kończy na podsumowaniu i wnioskach. Rozprawa doktorska składa się z sześciu rozdziałów.
Rozdział 1 przedstawia ogólne wprowadzenie do rozprawy doktorskiej i SIF. W rozdziale tym przedstawiono cele i hipotezy badawcze pracy. Scharakteryzowano rodzaje i źródła sygnałów SIF emitowanych przez rośliny. Ponadto, opisano również szczegółowo kampanię lotniczą HyPlant oraz przyjęte metody badawcze pozwalające na weryfikacje postawionych hipotez.
Rozdział 2 dotyczy kompleksowego przeglądu stanu najnowszej wiedzy dotyczącego badań nad SIF na poziomie „canopy" (TOC) mierzonych za pomocą systemów naziemnych, czy też z wykorzystaniem różnych platform takich jak drony, samoloty i satelity. Przegląd literatury światowej obejmuje prace dotyczące technik pomiarowych SIF, algorytmów szacowania SIF, modelowania, przykłady zastosowania SIF oraz walidacji mierzonych sygnałów z uwzględnieniem różnych platform teledetekcyjnych wraz z charakterystyką ich obecnych ograniczeń.
Rozdział 3 przedstawia pierwsze zobrazowania lotnicze SIF dla obu pasm absorpcyjnych O_2 przy 687 nm i 760 nm uzyskane nad torfowiskiem Rzecińskim i otaczającymi go ekosystemami. W rozdziale tym pokazano również stopień zależności między sygnałami SIF w obu pasmach absorpcji O_2 a indeksami spektralnymi, które były związane z cechami strukturalnymi i funkcjonalnymi szaty roślinnej. Przedstawiono również zmienność sygnału SIF wraz z gradientem produktywności na torfowisku w skali ekosystemu i dla różnych zbiorowisk roślinnych.
Rozdział 4 przedstawia opis nowego modelu opartego na uczeniu maszynowym, który umożliwia symulację sygnałów SIF przy 687nm i 760nm w drodze aproksymacji krokowej na podstawie prostych wskaźników spektralnych (NDVI, SR, NDVIre, EVI, PRI) pozyskanych ze zobrazowania lotniczego z wykorzystaniem metod modelowania rozmytego i technik integracji danych. W rozdziale wykazano, że podejście oparte na modelach rozmytych może z dużą dokładnością przybliżać wartości sygnałów SIF w obu pasmach absorpcji O_2, a także może uchwycić strukturalną i funkcjonalną różnorodność roślinności w skali ekosystemu.
Rozdział 5 przedstawia znaczenie satelitarnych pomiarów spektrometrycznych bazujących na współczynnikach odbicia promieniowania i różnych indeksach roślinnych w szacowaniu produktywności pierwotnej brutto (GPP) i fotosyntezy netto (PsnNet) ekosystemów tropikalnych. W pracy przedstawiono wyniki analizy porównawczej różnych metod korelacji (tj. Pearsona, Spearmana i Kendalla) oraz nadzorowanych modeli uczenia maszynowego (tj. losowego lasu, warunkowego wnioskowania i kwantyli regresji) celem zbadania zgodności i możliwości

szacowania GPP oraz PsnNet na podstawie wskaźników spektralnych i reflektanci, w warunkach sezonowej zmienności roślinności strefy tropikalnej.

Rozdział 6 przedstawia syntezę i wnioski rozprawy doktorskiej. Ogólny wniosek wskazuje, że rozwijająca się nauka o SIF, obejmująca nowoczesne technologie teledetekcyjne, otworzyła nowe kierunki badań nad stanem roślinności ekosystemów lądowych i globalnego obiegu węgla, wraz z rozwojem nowych naziemnych systemów pomiarowych, takich jak FloXbox (JB Hyperspectral Devices GmbH, Germany) i PICCOLO-DOPPIO (The University of Edinburgh, UK), nowych przyrządów montowanych na platformach lotniczych jak np. HyPlant, czy rozwój i planowanie nowych misji kosmicznych, takich jak budowa satelity FLEX FLORIS Europejskiej Agencji Kosmicznej itp.

Wyniki rozprawy doktorskiej dostarczyły pierwszego eksperymentalnego dowodu na to, że poprzez fluorescencję chlorofilu w paśmie czerwonym (SIF_{687}) i dalekiej podczerwieni (SIF_{760}) możliwe jest uchwycenie ogromnej niejednorodności przestrzennej ekosystemów torfowisk, lasów i użytków zielonych, reprezentujących różną aktywność fotosyntetyczną, cechy biochemiczne i strukturalne zbiorowisk roślinnych, a tym samym umożliwienie oceny dużego zróżnicowania funkcjonalnego szaty roślinnej. Ponadto zaobserwowano, że opracowane techniki modelowania rozmytego, nazwane jako SIFfuzzy i SIFfuzzy-APAR, mogą przybliżyć z dużą dokładnością wartości sygnałów SIF w obu pasmach absorpcji O_2, a także są w stanie reprezentować różnorodność strukturalną i funkcjonalną szaty roślinnej. Badania te wykazały również, że różnice w warunkach meteorologicznych i środowiskowych mają wpływ na aktywność roślin, co znajduje odzwierciedlenie w mierzonych wartościach sygnałów spektralnych bazujących na obserwacjach satelitarnych, oraz istotnie wpływają na możliwość predykcji GPP i PsnNet za pomocą technik teledetekcyjnych.

Słowa Kluczowe: Fluorescencja indukowana promieniowaniem słonecznym (SIF), spektralne wskaźniki roślinne, *HyPlant*, obrazowanie lotnicze, modelowanie rozmyte, nauczanie maszynowe, produkcja pierwotna brutto (GPP), torfowisko, las, użytki zielone.

List of symbols and abbreviations

APAR	Absorbed photosynthetic active radiation
CAL/VAL	Calibration/Validation
cForest	Conditional inference forests
EC	Eddy Covariance
eFLD	Extended Fraunhofer Line Depth
ESA	European Space Agency
EVI	Enhanced vegetation index
fAPAR	Fraction of Absorbed Photosynthetically Active Radiation
FESC	Escape fraction of SIF photons
FLD	Fraunhofer Line Depth
FLEX	The FLuorescence EXplorer
GOME 2	Global Ozone Monitoring Experiment-2
GOSAT	Greenhouse Gases Observing Satellite
GPP	Gross primary productivity
iFLD	Improved Fraunhofer Line Depth
L7	Landsat 7 ETM+
L8	Landsat 8 OLI
LAI	Leaf Area Index
ML	Machine Learning
MODIS	Moderate Resolution Imaging Spectroradiometer
NASA	National Aeronautics and Space Administration
NDVI	Normalized difference vegetation index
NDVIre	Normalized difference red edge position
NIR	Near-infrared
NPP	Net primary productivity
NPQ	Non-photochemical quenching
OCO 2	Orbiting Carbon Observatory-2
OLI	Operational Land Imager
OOB	Out of bag error
PAR	Photosynthetically active radiation
PRI	Photochemical Reflectance Index
QRF	Quantile regression forests
RF	Random Forest
RS	Remote Sensing
RTM	Radiative Transfer Modelling
S2	Sentinel 2
SFM	Spectral Fitting Method
SIF	Sun-induced chlorophyll fluorescence
SIF_{687}	Sun-induced chlorophyll fluorescence at 687nm
SIF_{760}	Sun-induced chlorophyll fluorescence at 760nm
SIF_{fuzzy}	Fuzzy simulated Sun-induced chlorophyll fluorescence

$SIF_{fuzzy\text{-}APAR}$	Combined fuzzy and Absorbed photosynthetic active radiation simulated Sun-induced chlorophyll fluorescence
SNR	Signal to Noise Ratio
SR	Simple Ratio
SVD	Singular Vector Decomposition
SVIs	Spectral Vegetation Indices
SWAMP	Spectrometry of a Wetland and Modelling of Photosynthesis
SWIR	Shortwave Infrared
TOA	Top-of-Atmosphere
TOC	Top-of-canopy
UAV	Unmanned aerial vehicle
USGS	United States Geological Survey
VIs	Vegetation Indices
VNIR	Visible Near Infrared

CHAPTER 1
General Introduction

1. Introduction

Remote Sensing (RS) of Sun-induced fluorescence or solar-induced chlorophyll fluorescence (SIF) is an advanced growing front in terrestrial ecosystem science and in agricultural studies that have strong capabilities and emerges as a unique signal to monitor global vegetation status, encompassing its structural and functional diversity from the canopy to ecosystem-scales (Bandopadhyay et al., 2020; Mohammed et al., 2019). Measurement and estimation of SIF using different remote sensing (RS) platforms greatly enhanced and significantly increased the multiple opportunities to monitor, quantify, and model the plant photosynthetic activity in a more detailed nature (Yang et al., 2018). The importance and popularity of SIF, is not only restricted to the remote sensing communities dealing with plants and ecosystems but also beneficial for those working in broader fields related to plant physiology, biophysics, biochemistry, and agricultural community (Bandopadhyay et al., 2020). Moreover, the strong agreement between SIF and gross primary productivity (GPP) enriched the importance of SIF as a prime indicator for terrestrial photosynthesis and global carbon cycle reported by several studies such as Damm et al., 2010; Gentine and Alemohammad, 2018; Smith et al., 2018; Walther et al., 2016. Scientists also consider the novel SIF signal as a prime indicator of climate change and its significant impact on terrestrial vegetation and crop production (Kimm et al., 2021).

The novel SIF signal emitted from the core of plant photosynthetic machinery was captured in the spectral range of 640 nm to 800 nm (Buschmann et al., 2001). The plant molecules (plant-derived compounds and related genes) absorb solar energy as a form of photons and on the absorption of photons, the plant molecules reached their excited state. However, such exciting molecules do not want to stay excited about the long term. So, the highly energetic excited molecules release energy through vibration, relaxation and photon emission, which is called SIF (Bandopadhyay et al., 2020; Narayan et al., 2012). SIF originates from the initial reactions in Photosystem (PS) and occurs at the wavelengths between 650 nm and 780 nm, with the first peak at 690 nm (SIF_{690}), whereas PS I fluorescence occurs in the far-red/near-infrared spectrum (>700 nm) with a peak at 760 nm (SIF_{760}) (Bandopadhyay et al., 2020; Govindjee, 2004). The full spectrum of SIF covers the wavelengths between visible (VIS) to near-infrared (NIR) spectrum from 640–800 nm. Both PS II and PS I operate in sequential order and are commonly recognized by two peak signals identified by their usual wavelength positions at SIF_{690} and SIF_{760} for PS II and PS I, respectively (Buschmann et al., 2001; Govindjee, 2004).

The advancement of RS technologies offers unprecedented opportunities to monitor, and model the terrestrial vegetation in a vivid manner. The development of state-of-the-art RS-based opportunities helps to understand the status of vegetation, its phenology, and its functional activities in real-time as well as in time-series. The traditional RS-based observations on terrestrial vegetation and agriculture solely rely on the canopy reflectance spectra at different spectral channels. Spectrally derived vegetation indices (VIs) are the most common practice on vegetation remote sensing. Over time, several spectrally derived VIs have been developed to represent

the vegetation traits such as greenness content (Rahaman et al., 2017), leaf area (Gitelson et al., 2014), red-edge position (Dong et al., 2019), biomass content (Kumar and Mutanga, 2017), water content (Cohen, 1991), zeaxanthin content (Harris et al., 2014), etc. However, such vegetation traits based on the spectral indices are not sensitive enough to monitor the short-term dynamics of vegetation functionalities. The photosynthetic process caused by different environmental conditions (i.e., incident irradiance, temperature, etc.) or stress factors impacting plant physiology is not exposed enough by such spectral indices. As the SIF signal is strongly connected with the core of the photosynthetic-process, the short-term changes in plant physiological process can be easily captured by SIF signals compared to spectral indices. SIF is highly accomplished with estimating and detecting more accurate carbon assimilation rates and earlier stress symptoms rather than normal reflectance spectra and vegetation indices (Campbell et al., 2008). Furthermore, SIF signal is highly dynamic in nature and very sensitive towards the minor changes of plant physiological conditions, which can be easily detectable by the modern RS technologies in a real-time manner.

Narrow-band hyperspectral imaging spectrometers are rapidly evolving in the contemporary era and provide unique opportunities for mapping and modeling of terrestrial vegetation and its functioning through novel SIF signal. Advanced features of hyperspectral spectrometers with fine spectral resolutions (<0.1 nm) have unique capabilities to capture the weak signals around 640 nm to 800 nm needed to retrieve SIF. Development of modern SIF retrieval physics-based methods like improved- Fraunhofer line depth (iFLD), full-spectrum Spectral Fitting Method (SFM), or statistical methods like singular value decomposition (SVD) facilitates the improved and accurate estimations of SIF signals at both O_2 absorption bands through modern remote sensing techniques (Bandopadhyay et al., 2020; Mohammed et al., 2019). The estimation of SIF signal from radiances is mainly recorded at the top-of-canopy (TOC) or the top-of-atmosphere (TOA) level, which typically constitutes 1–5% of the reflected radiation in the red and NIR regions as a very weak signal. The traditional methods for estimating SIF signal exploit the regions of the atmospheric spectrum where the incident irradiance is strongly reduced due to the absorption in the Earth's atmosphere (Rossini et al., 2010). The two peaks are characterized by the two telluric oxygen absorption features, namely O_2A at 760.4 nm and O_2B at 687.0 nm. To capture such narrow atmospheric absorption bands, spectrometers should contain fine full width at half maximum (FWHM) of 1–5 nm or ultrafine (FWHM < 1 nm) spectral resolutions in any detectable spectrometer based on RS platform. Thus, recent development of advanced high-resolution spectrometers with good accuracies and low noise explored the scope of SIF estimation at both O_2 absorption bands using high-resolution passive spectrometers on the ground, UAV, airborne, and satellite-based RS platforms enriched our understanding of terrestrial vegetation and its functionalities.

1.1 Significance of the work in the contemporary era

Global changes in the Earth's ecological systems due to climate change, frequent heat waves, extreme precipitation, biodiversity loss, artificially increased nitrogen (N) inputs, and inadequate phosphorus (P) supply forecasts that the future is unprecedented and uncertain for global human civilization. Such modifications in ecology and ecosystem services posing a rapidly increasing threat to global food production and sustainability worldwide. On the other hand, the global population rising rapidly and this trend will continue for upcoming decades. Projections indicate a 95% rise of the global population that steeply rise the increasing demand on the resources such as food, and water, disturbed living standards, which will stress upon terrestrial ecosystems and their inherent productivity and resilience (Rohr et al., 2019).

Observation and accurate quantification of photosynthetic activity of terrestrial vegetation from space are still challenging and often the results of estimations are very biased. Traditional and available spectral observations are based only on TOC reflectance spectra but they are not directly linked to the core of plant photosynthetic activities. Chlorophyll fluorescence is the most direct technique and measurable signal originating from the core of plant photosynthetic machinery and provides new avenues for accessing the dynamics of actual photosynthesis at various spatial scales. This unique signal has more potential to monitor actual photosynthesis compared to current observations based on passive reflectance spectra in the optical range. Moreover, the uptake of CO_2 through photosynthesis and the release of CO_2 by respiration and other processes maintains the global biogeochemical balance. According to the Intergovernmental Panel on Climate Change (IPCC) special report on global warming in 2018 and in IPCC report 2021 (IPCC report 2021, AR6), the post-industrialization phase increased the carbon emission compared to the pre-industrialization phase further contributed by fossil-fuel combustion, massive deforestation, changes in land-use pattern, intensive cultivation, and logging (Wigley et al., 2019). In this scenario, a huge uncertainty is developed over the time on global sustainability and terrestrial functionality that demands an urgent need to access the role of vegetation on the global carbon cycle. Studies have already established a strong agreement between the global carbon cycle and plant fluorescence activity (Lee et al., 2015; Running et al., 2004) that immensely enriched the existing understanding of the carbon cycle. Additionally, the HyPlant sensor data, used in this thesis, is the airborne demonstrator of the ESA Fluorescence Explorer (FLEX) Sentinel 3 FLORIS satellite (Drusch et al., 2017) considered as a significant contribution towards the upcoming satellite mission as well as for calibration and validation (CAL/VAL) activities.

1.2 Research Scope and Objectives

The main objective of this thesis is to assess the Sun-induced fluorescence (SIF) and reflectance (R) of different ecosystems through ground, airborne and satellite remote sensing techniques. The significance of SIF has been well recognized by scientists and researchers in the domain of vegetation and agricultural sciences. However, the exploration of SIF signals over heterogeneous ecosystems such as for example peatlands, where spectral diversity is rich and complex, have not been explored so much. There is a significant knowledge gap, about the sensitivity of SIF signals and its reaction over spectrally diverse and complex mosaic of different ecosystems and this thesis aims at filling this gap with the new knowledge.

In recent years, the research explored the classical hyperspectral data analysis to assess the diversity of peatland vegetation (Erudel et al., 2017). Studies have been demonstrated the potential of hyperspectral reflectances that enriched the understanding of ecological patterns of peatland and other homogeneous surfaces like forests, grasslands and croplands. Time series of phenological changes, gradient mapping, structural and functional traits have been also explored by hyperspectral reflectances over both homogeneous and heterogeneous landscapes. However, comparatively unique SIF signals obtained through narrow-band hyperspectral imaging spectrometers originating from photosynthetic machinery have been not used yet to monitor and analyze the heterogeneous peatland and mosaic of different ecosystems. Moreover, the implementation of narrow band SIF signals on airborne imaging spectroscopy is an extremely new technique in support of future space missions. Now-a-days the implementation of spaceborne SIF signals over various ecosystems is a regular practice compared to modern RS platform-based observations such as airborne, UAV, or with advanced high-resolution ground spectrometers. To implement and recognize the applications of potential SIF signals and to explore its full spectrum using different RS observations, a complete document of existing SIF studies is highly demanded and hence it is summarised and discussed in the thesis.

In this research for the first time, telluric oxygen absorption bands of SIF around 760 nm and 687 nm over heterogeneous peatland and surrounding ecosystems have been retrieved from airborne imaging spectroscopy data. Additionally, structural and functional traits along with the biochemical components of peatland and surrounded ecosystems have been also analyzed through airborne imaging spectroscopy obtained SIF signals and spectral reflectances. Therefore, the first hypothesis formulated that *novel SIF signals have a direct agreement with vegetation traits, however, this agreement may vary from plant community scale to ecosystem scale.*

Furthermore, machine-learning-based fuzzy modelling techniques have been implemented for the first time to approximate the SIF signals at both oxygen absorption bands from vegetation traits obtained from spectral reflectances using airborne imaging spectroscopy datasets. The second hypothesis formulated that *vegetation traits can be used to approximate SIF at both oxygen absorption bands and can also replicate SIF signals over different ecosystems in agreement with the original (measured) SIF.*

The predictor variables for gross primary productivity (GPP) and net-photosynthesis (PsnNet) are highly dynamic in nature influenced by the anomalies that occurred due to seasonal and environmental variabilities. Such dynamic nature of vegetation functional activities can be possible to measure through satellite derived reflectance spectra. In this research, such anomalies of predictor variables for GPP and PsnNet in terms of several vegetation traits obtained through spaceborne spectral reflectances have been identified using different supervised machine learning models and correlation-based statistical approaches. The third hypothesis formulated that *seasonal and environmental anomalies cannot only impacted the GPP and PsnNet prediction process but also the correlations with vegetation indices.*

Therefore, based on the above-discussed research scopes and hypothesizes the following specific objectives were identified in this thesis:

(1) To evaluate the current potential application of SIF, conducting in-depth survey, review, and interpretation of existing SIF studies based on the ground, airborne, UAV, and spaceborne observations, in order to identify the current knowledge gap, associated limitations and challenges of existing SIF studies (**Investigated in chapter 2, Publication 1**)

(2) To retrieve the first airborne SIF maps at both oxygen absorption bands (SIF_{760} and SIF_{687}) of heterogeneous peatland and surrounding ecosystems. Also, exploration and analysis of SIF_{760} and SIF_{687} signals obtained from different managed and natural ecosystems over homogeneous (forest, grassland, etc.) as well as from heterogeneous (peatland) ecosystems using airborne imaging spectroscopic data (**Investigated in chapter 3, Publication 2**)

(3) To understand and compare the inter-relationship between spectral vegetation indices and vegetation biophysical parameters with SIF_{760} and SIF_{687} signals over peatland and surrounding ecosystems from plant community scale to ecosystem scale. (**Investigated in chapter 3, Publication 2**).

(4) To develop a proxy of SIF signals from simple spectral vegetation indices using airborne imaging spectroscopic data. Furthermore, step-wise approximation of the novel SIF_{760} and SIF_{687} signals from different vegetation traits in terms of spectral indices using the fuzzy model and airborne spectrometry (**Investigated in chapter 4, Publication 3**)

(5) To understand the seasonal uncertainties in GPP and PsnNet prediction process from satellite derived reflectenace spectra as well as to compare and understand the interlink with several spectral vegetation indices and tasselled cap transformations, through the implementation of different correlation methods (i.e. Pearson, Spearman, and Kendall rank) as well as through different supervised machine learning models (i.e. Random forest-RF, Conditional inference forests- cForest, and Quantile regression forests- QRF) (**Investigated in chapter 5, Publication 4**).

1.3 Thesis Outline

The content of this thesis is structured into six chapters. The core of this thesis (Chapters 2-5) is based on a series of four-peer reviewed publications. Each chapter is outlined here with the basic summaries and connecting its relationship with other relevant works.

Chapter 1 deals with the general introduction of SIF signals and its application with hyperspectral remote sensing technologies over terrestrial vegetation. The need for this work in the current time along with the research scope, hypothesis, and objectives of this thesis are provided in this chapter.

Chapter 2 addresses the first objective of the thesis. It reviews the existing SIF studies based on the ground, airborne, UAV, and spaceborne remote sensing techniques. Along with the critical analysis. This chapter provides limitations of such studies and explored the knowledge gaps and future scopes.

Chapter 3 investigates the second objective of this thesis. It presents the first airborne SIF maps at 760 nm and 687 nm over heterogeneous peatland ecosystems and their surrounding ecosystems (forest and grassland). Interpretation and interlinks between SIF signals with vegetation traits and biophysical parameters from ecosystem to plant community scales are reported in this chapter.

Chapter 4 focuses on development of alterative methodological approach of SIF estimation. The chapter deals with the fuzzy modelling technique that can simulate the novel SIF signals from airborne derived spectral vegetation indices in agreement with original SIF signals. The step-wise approximation of SIF_{760} and SIF_{687} from different vegetation traits is also addressed in this chapter.

Chapter 5 addresses the impact of seasonal and environmental anomalies in the GPP and PsnNet prediction process based on the comparisons of correlation and supervised machine learning models using MODIS Terra and Landsat 8 OLI datasets over a tropical mixed ecosystem.

Finally, **chapter 6** presents the synthesis of this thesis with conclusions, main findings, and suggestions for future work.

2. Materials and Method

2.1 Site Description

The core part of the research work portrayed in this thesis has been conducted over the Rzecin (POLWET) peatland area located in the western part of Poland. There are two main justifications behind the selection of this study area: (1) peatland is a unique ecosystem composed of wide species diversity and has around one-third of the terrestrial carbon stored in it that plays a crucial role in the global carbon cycle; (2) the implementation and observation of novel SIF signals over the peatland ecosystem are very new and contemporary with the highest challenges of complex

spectral diversity originated from mixed-species populations. The geographical extension of Rzecin peatland located in between 52°45′N latitude, 16°18′E longitude, with 54 m a.s.l. extended over an area of 114 hectares. The Rzecin peatland is extremely valuable from flora and fauna diversity and conservation perspectives that it comes under the Natura 2000 network of protected areas covering Europe's most valuable and threatened species and habitats ("Torfowisko Rzecinskie" PLH300019). This research is not only focused on the heterogeneous peatland, but also includes surrounding homogeneous patches of pine forest, grassland, deforestation sites, and cropland.

More details about the Rzecin study site along with the locational map is provided in chapter 3 and chapter 4.

The study portrayed in chapter 5 was carried out in and around the Gorumara National Park (GNP) of Dooars region, West-Bengal, India. The study area enriched with mixed ecosystems like forest, tea gardens, croplands, mountainous vegetation, terai grassland, swampland, and rivers that comes under humid subtropical climate.

More details about the GNP and its surrounding study site along with the locational map is provided in chapter 5.

2.2 Airborne Hyperspectral Measurements

On 11th July 2015, HyPlant airborne campaign have been organised and funded by the European Space Agency (ESA) under Fluorescence Explorer FLEX-EU mission, European Facility for Airborne Research (EUFAR) and Cost Action OPTIMISE (ES1903) at the Rzecin peatland in Poland. This airborne campaign have been acknowledged as *Sprectrometry of a wetland and modelling of photosynthesis: hyperspectral airborne reflectance and fluorescence in education and research* (SWAMP) campaign and SWAMP summer school that involved group of students, researchers, scientists, professors from different institutions of Europe. Different peoples were involved in different activities from field data collection, airborne data collection, calibration activities etc. and most of them have been listed as co-authors of the publication 2 and their contribution is acknowledged in the paper.

HyPlant airborne imaging spectrometer has been flown over the Rzecin peatland site, installed on a Cessna Grand Caravan C208B (a turboprop aircraft) owned and operated by CzechGlobe, Czech Republic. At a flying altitude of 690 meters, six flight lines were acquired between 09:50 to 10:46 and 13:10 to 13:55 resulting in the images in a spatial resolution of 1 × 1 m per pixel. The airborne HyPlant imaging spectrometer constellated with two push-broom sensors: (1) a broadband dual-channel module (DUAL module) which captured surface reflected radiance with the spectral resolution of 3 nm in the visible and near-infrared (VIS/NIR) regions and about 10 nm in the short-wave infrared (SWIR) region; it covered a spectral range of 370–2500 nm, and (2) narrow-band spectrometer (FLUO module) which covered the red and far-red region of the electromagnetic spectrum ranges from 670 to 800 nm, with a spectral resolution of 0.25 nm. DUAL module outputs have been used to

acquire the reflectances followed by the development of spectral VIs, whereas the FLUO module provides SIF_{760} and SIF_{687} images.

The atmospheric corrections have been conducted through ATCOR (Atmospheric & Topographic Correction model, ReSe Applications Schläpfer, Langeggweg, Switzerland) based on 5S radiative transfer model (RTM) to obtain Top-of-Canopy (TOC) reflectance and radiance values. Furthermore, topographic corrections, geo-rectifications of the airborne images have been conducted using the CaliGeo toolbox (SPECIM, Oulu, Finland). The data processing chain and calculations needed to retrieve reflectance and SIF from airborne data has been done by Dr. Patrick Rademske from Plant Sciences, Forschungszentrum Jülich, Germany and Dr. Sergio Cogliati from Department of Earth and Environmental Sciences, University of Milano-Bicocca, Italy within the FLEX-EU (ESA) project.

More details and specifications about the airborne hyperspectral measurement are provided in chapter 3 and chapter 4.

2.3 Field Hyperspectral Measurements

Two spectrometers within HR4000 (OceanOptics, Largo, FL, USA) covering different wavelength ranges were used to estimate TOC reflectance and SIF. One of them operated in the visible and near-infrared region (350–1050 nm) spectral range with a full-width half maxima (FWHM) of 1 nm have been utilized to compute the radiance and spectral VIs. Another spectrometer covered the spectral range 650–840 nm with a spectral resolution of 0.2 nm (FWHM) and has been utilized to estimate the SIF signals at both oxygen absorption bands at 760 nm (SIF_{760}) and 687 nm (SIF_{687}). Both the spectrometers were spectrally calibrated with standards using CAL-2000 mercury argon lamp, OceanOptics, Largo, FL, USA whereas radiometric calibration was inferred from cross-calibration measurements performed with a reference calibrated FieldSpec spectrometer (Analytical Spectral Device, Boulder, CO, USA). These measurements has been done and data were processed by Dr. Tommaso Julitta from Department of Earth and Environmental Sciences, University of Milano-Bicocca, Italy.

Other technical details of the field hyperspectral measurements are provided in chapter 3.

The field hyperspectral measurements have been carried out on 11th July 2015 (same day and time of the airborne measurement) at midday from 11:00 to 14:20 solar time under clear sky conditions at nine plots (V1–V9). The the nine ground measurement plots were located along the main boardwalk in the South-North direction and they were representing different vegetation—i.e., from *Carex* dominated communities and *Typha* dominated communities (high biomass of vascular plants) to *Sphagnum* dominated communities (low biomass of vascular plants) dominated groups. More details about the vegetation composition of nine measurement plots with locational details have been provided in Figure 2 and Table 2 from Chapter 3 (publication 2).

Additionally, on the day of 11th July 2015, Leaf Area Index (LAI), Photosynthetically active radiation (PAR), and Fraction of Absorbed Photosynthetically Active Radiation (fAPAR) have been measured with BF5 sensor (DELTA-T, UK) over the Rzecin peatland.These measurements has been done by Dr Karolina Sakowska from Institute of BioEconomy, Italian National Research Council. Weather data have been acquired from the weather station placed in the middle of the Rzecin peatland.

2.4 Computation of vegetation indices

Several spectral vegetation indices representing different vegetation traits related to plant physiology, chemical composition, structure, xanthophyll pigments, and water content were calculated from TOC reflectances acquired from the HyPlant DUAL-channel module (indicated in 2.2 section) as well as from hyperspectral radiometers used for the ground-truth measurements (indicated in 2.3 section). VIs like Normalized Difference Vegetation Index (NDVI) and Simple Ratio (SR) representing greenness content, Photochemical Reflectance Index (PRI) representing xanthophyll content, Normalized Difference red-edge position (NDVIre) representing vegetation red-edge position, Enhanced Vegetation Index (EVI) have been calculated based on equations provided in chapter 3 and chapter 4.

2.5 Retrieval of SIF through Spectral Fitting Method (SFM)

The far-red SIF (SIF_{760}) and red SIF (SIF_{687}) maps over the Rzecin peatland have been computed based on Spectral Fitting Method (SFM). Both airborne SIF maps and ground SIF have been estimated using the SFM method. Due to the prototyped nature of the system and established processing chain by ESA FLEX mission, the SFM based SIF maps have been processed by Dr. Sergio Cogliati from University of Milano-Bicocca, Italy. I have calibrated and rescaled the SFM maps over the Rzecin peatland in my study broadly discussed in section 2.6 of the chapter 3 (publication 2).

The SFM algorithm requires high spectral resolution-based measurements both from the ground and airborne sensors. The technique depends on the analysis of the radiance spectra in high spectral resolution at the O_2 absorption bands (O_2-A and O_2-B at 760 and 687 nm, respectively), where the fluorescence contribution to the overall canopy emerging radiance was larger. More details about the SFM method have been discussed by Cogliati et al., 2015.

The fluorescence retrieval approach consisted of two main components: i) The atmospheric radiative transfer was computed through MODTRAN5 (MODerate resolution atmospheric TRANsmission) Radiative Transfer (RT) model; while ii) the decoupling of fluorescence radiances and reflectance was achieved based on the spectral fitting technique. The pre-processing steps include radiometric and spectral calibration, correction of detector non-linearity, and the deconvolution of the

instrument point-spread-function (PSF). The retrieval was carried out through the comparison of the HyPlant and the forward-modelled radiance spectrum in defined spectral windows at the sensor level. The SFM module implemented in the airborne HyPlant datasets is based on the third-order polynomial functions and Pseudo-Voigt functions to approximate reflectance and fluorescence spectral behaviour. SFM starts the preliminary estimation of fluorescence values inside the O_2 absorption bands for faster convergence and provides the outputs with the full spectrum of fluorescence.

The SFM algorithm was developed for the FLEX FLORIS (ESA) satellite, however, it was implemented for HyPlant airborne datasets to demonstrate it reliability and applicability. The TOA radiance is first converted to TOC radiance through the atmospheric correction process, and further, the bottom of atmosphere radiance spectra deconvoluted into the contributions of fluorescence and reflected light fluxes. The fluorescence emission peaks of red SIF at 687 nm and far-red SIF at 760 nm are modelled through the combination of different functions like Gaussian, Lorentzian, and Voigt. Through the implementation of the least-squares non-linear curve fitting optimization process, it minimizes the processing time.

More details about the SFM function and its implementation for SIF retrieval from HyPlant data were provided in chapter 3.

2.6 Fuzzy Modelling

The fuzzy logic simulations are similar as people make inferences and decisions based on observations. Fuzzy assemble flexible combinations of weighted maps and possible to readily implemented using spatial modelling language. The theory and concept of fuzzy logic were first implemented by Zadeh, 1965 and was widely accepted by other scientific fields applications in hydrology, geomorphology, environmental. The fuzzy technique considers the degree of membership by the input variables through the membership function techniques. The membership sets of the different input variables ranging between 0 and 1 reflecting a certain degree of the membership where 0 represents no membership and 1 represents high membership. Furthermore, it employs the assimilation of memberships to obtain the best possible outcomes through five possible overlay operators such as fuzzy And, fuzzy Or, fuzzy Product, fuzzy Sum, and fuzzy Gamma.

However, the implementation of fuzzy logic in the approximation of SIF signals using airborne imaging spectroscopy is very new and has been applied for the first time. In this thesis, the fuzzy modelling technique was used for the first time to approximate the SIF signals at far-red SIF (SIF_{760}) and red SIF (SIF_{687}) through several combinations of the vegetation traits. First, the vegetation traits in terms of spectral VIs were transformed to membership functions and further several iterations were run with different combinations of the spectral VIs using fuzzy Gamma operator. More details about the fuzzy modelling technique implemented in this thesis are discussed in chapter 4.

2.7 Supervised Machine Learning models

Supervised machine learning (ML) modelling techniques becomes popular in recent time that offers unprecedented robust applications in all aspects of Earth observation science. Such ML algorithms have become widely accepted by the Earth observation community because of their high-precision accuracy and less processing time. The implementation of such ML techniques to satellite derived reflectance based spectral indices, tasseled cap transformations for GPP and PsnNet prediction process is a new and modern technique. In this thesis, three decision based supervised ML models namely random forest (RF), conditional inference forests (cForest), and quantile regression forests (QRF) were compared to identify and explore the prediction process of GPP and PsnNet under the Indian seasonal variability from several VIs, spectral bands, and tasselled cap transformations using MODIS and Landsat 8 OLI data. To train and evaluate the models the entire dataset was divided into 70% for training and 30% for testing in all three prediction models. The RF model is a meta estimator that develops a number of decision trees based on different sub-samples of the dataset and the final prediction is computed by the averaging of the decision trees. The cForest model considers a more accurate and better estimator than RF in terms of accuracy as it uses out-of-bag (OOB) data that ensures more insight and higher accuracy. The QRF model considers the quantile distributions (0.05 percentile to 0.95 percentile) of predictor variables to predict the target through building RF.

Further details about RF, cForest, and QRF were discussed in chapter 5.

References

Arias, P., Bellouin, N., Coppola, E., Jones, R., Krinner, G., Marotzke, J., Naik, V., Palmer, M., Plattner, G.K., Rogelj, J. and Rojas, M., 2021. Climate Change 2021: The Physical Science Basis. Contribution of Working Group14 I to the Sixth Assessment Report of the Intergovernmental Panel on Climate Change; Technical Summary.

Bandopadhyay, S., Rastogi, A., Juszczak, R., 2020. Review of top-of-canopy sun-induced fluorescence (Sif) studies from ground, uav, airborne to spaceborne observations. Sensors (Switzerland) 20, 1144. https://doi.org/10.3390/s20041144

Bandopadhyay, S., Rastogi, A., Rascher, U., Rademske, P., Schickling, A., Cogliati, S., Julitta, T., Arthur, A. Mac, Hueni, A., Tomelleri, E., Celesti, M., Burkart, A., Strózecki, M., Sakowska, K., Gabka, M., Rosadziński, S., Sojka, M., Iordache, M.D., Reusen, I., Van Der Tol, C., Damm, A., Schuettemeyer, D., Juszczak, R., 2019. Hyplant-derived Sun-Induced Fluorescence-A new opportunity to disentangle complex vegetation signals from diverse vegetation types. Remote Sens. 11, 1691. https://doi.org/10.3390/rs11141691

Buschmann, C., Langsdorf, G., Lichtenthaler, H.K., 2001. Imaging of the blue, green, and red fluorescence emission of plants: An overview. Photosynthetica. https://doi.org/10.1023/A:1012440903014

Campbell, P.K.E., Middleton, E.M., Corp, L.A., Kim, M.S., 2008. Contribution of chlorophyll fluorescence to the apparent vegetation reflectance. Sci. Total Environ. 404, 433-439. https://doi.org/10.1016/j.scitotenv.2007.11.004

Cogliati, S., Verhoef, W., Kraft, S., Sabater, N., Alonso, L., Vicent, J., Moreno, J., Drusch, M., Colombo, R., 2015. Retrieval of sun-induced fluorescence using advanced spectral fitting methods. Remote Sens. Environ. 169, 344-357. https://doi.org/10.1016/j.rse.2015.08.022

Cohen, W.B., 1991. Response of vegetation indices to changes in three measures of leaf water stress. Photogramm. Eng. Remote Sens. 57, 195–202.

Damm, A., Elber, J., Erler, A., Gioli, B., Hamdi, K., Hutjes, R., Kosvancova, M., Meroni, M., Miglietta, F., Moersch, A., Moreno, J., Schickling, A., Sonnenschein, R., Udelhoven, T., van der Linden, S., Hostert, P., Rascher, U., 2010. Remote sensing of sun-induced fluorescence to improve modeling of diurnal courses of gross primary production (GPP). Glob. Chang. Biol. 16, 171-186. https://doi.org/10.1111/j.1365-2486.2009.01908.x

Dong, T., Liu, J., Shang, J., Qian, B., Ma, B., Kovacs, J.M., Walters, D., Jiao, X., Geng, X., Shi, Y., 2019. Assessment of red-edge vegetation indices for crop leaf area index estimation. Remote Sens. Environ. 222, 133–143. https://doi.org/10.1016/j.rse.2018.12.032

Drusch, M., Moreno, J., Del Bello, U., Franco, R., Goulas, Y., Huth, A., Kraft, S., Middleton, E.M., Miglietta, F., Mohammed, G., Nedbal, L., Rascher, U., Schuttemeyer, D., Verhoef, W., 2017. The FLuorescence EXplorer Mission Concept-ESA's Earth Explorer 8. IEEE Trans. Geosci. Remote Sens. 55, 1273-1284. https://doi.org/10.1109/TGRS.2016.2621820

Erudel, T., Fabre, S., Houet, T., Mazier, F., Briottet, X., 2017. Criteria Comparison for Classifying Peatland Vegetation Types Using In Situ Hyperspectral Measurements. Remote Sens. 9, 748. https://doi.org/10.3390/rs9070748

Gentine, P., Alemohammad, S.H., 2018. Reconstructed Solar-Induced Fluorescence: A Machine Learning Vegetation Product Based on MODIS Surface Reflectance to Reproduce GOME-2 Solar-Induced Fluorescence. Geophys. Res. Lett. 45, 3136-3146. https://doi.org/10.1002/2017GL076294

Gitelson, A.A., Peng, Y., Huemmrich, K.F., 2014. Relationship between fraction of radiation absorbed by photosynthesizing maize and soybean canopies and NDVI from remotely sensed data taken at close range and from MODIS 250m resolution data. Remote Sens. Environ. 147, 108–120. https://doi.org/10.1016/j.rse.2014.02.014

Govindjee, 2004. Chlorophyll a Fluorescence: A Bit of Basics and History In: Papageorgiou G, Govindjee (eds.), Chlorophyll a Fluorescence: a Signature of Photosynthesis. Springer Dordr. 1–42.

Harris, A., Gamon, J.A., Pastorello, G.Z., Wong, C.Y.S., 2014. Retrieval of the photochemical reflectance index for assessing xanthophyll cycle activity: A comparison of near-surface optical sensors. Biogeosciences 11, 6277–6292. https://doi.org/10.5194/bg-11-6277-2014

Kimm, H., Guan, K., Burroughs, C.H., Peng, B., Ainsworth, E.A., Bernacchi, C.J., Moore, C.E., Kumagai, E., Yang, X., Berry, J.A., Wu, G., 2021. Quantifying high-temperature stress on soybean canopy photosynthesis: The unique role of sun-induced chlorophyll fluorescence. Glob. Chang. Biol. 27, 2403–2415. https://doi.org/10.1111/gcb.15603

Kumar, L., Mutanga, O., 2017. Remote sensing of above-ground biomass. Remote Sens. 9, 1–8. https://doi.org/10.3390/rs9090935

Lee, J.E., Berry, J.A., van der Tol, C., Yang, X., Guanter, L., Damm, A., Baker, I., Frankenberg, C., 2015. Simulations of chlorophyll fluorescence incorporated into the Community Land Model version 4. Glob. Chang. Biol. 21, 3469-3477. https://doi.org/10.1111/gcb.12948

Mohammed, G.H., Colombo, R., Middleton, E.M., Rascher, U., van der Tol, C., Nedbal, L., Goulas, Y., Pérez-Priego, O., Damm, A., Meroni, M., Joiner, J., Cogliati, S., Verhoef, W., Malenovský, Z., Gastellu-Etchegorry, J.P., Miller, J.R., Guanter, L., Moreno, J., Moya, I., Berry, J.A., Frankenberg, C., Zarco-Tejada, P.J., 2019. Remote sensing of solar-induced chlorophyll fluorescence (SIF) in vegetation: 50 years of progress. Remote Sens. Environ. 231, 111177. https://doi.org/10.1016/j.rse.2019.04.030

Narayan, A., Misra, M., Singh, R., 2012. Chlorophyll Fluorescence in Plant Biology, in: Biophysics. pp. 171-192. https://doi.org/10.5772/35111

Rahaman, K.R., Hassan, Q.K., Ahmed, M.R., 2017. Pan-sharpening of landsat-8 images and its application in calculating vegetation greenness and canopy water contents. ISPRS Int. J. Geo-Information 6, 168. https://doi.org/10.3390/ijgi6060168

Rohr, J.R., Barrett, C.B., Civitello, D.J., Craft, M.E., Delius, B., DeLeo, G.A., Hudson, P.J., Jouanard, N., Nguyen, K.H., Ostfeld, R.S. and Remais, J.V., 2019. Emerging human infectious diseases and the links to global food production. Nature sustainability, 2(6), pp.445-456.

Rossini, M., Meroni, M., Migliavacca, M., Manca, G., Cogliati, S., Busetto, L., Picchi, V., Cescatti, A., Seufert, G., Colombo, R., 2010. High resolution field spectroscopy measurements for estimating gross ecosystem production in a rice field. Agric. For. Meteorol. 150, 1283-1296. https://doi.org/10.1016/j.agrformet.2010.05.011

Running, S.W., Nemani, R.R., Heinsch, faith ann, Zhao, M., Reeves, M., Hashimoto, H., 2004. A Continuous Satellite-Derived Measure of Global Terrestrial Primary Production. Bioscience 54, 547. https://doi.org/10.1641/0006-3568(2004)054[0547:acsmog]2.0.co;2

Smith, W.K., Biederman, J.A., Scott, R.L., Moore, D.J.P., He, M., Kimball, J.S., Yan, D., Hudson, A., Barnes, M.L., MacBean, N., Fox, A.M., Litvak, M.E., 2018. Chlorophyll Fluorescence Better Captures Seasonal and Interannual Gross Primary Productivity Dynamics Across Dryland Ecosystems of Southwestern North America. Geophys. Res. Lett. 45, 748-757. https://doi.org/10.1002/2017GL075922

Walther, S., Voigt, M., Thum, T., Gonsamo, A., Zhang, Y., Köhler, P., Jung, M., Varlagin, A., Guanter, L., 2016. Satellite chlorophyll fluorescence measurements reveal large-scale decoupling of photosynthesis and greenness dynamics in boreal evergreen forests. Glob. Chang. Biol. 22, 2979-2996. https://doi.org/10.1111/gcb.13200

Wigley, T.M.L., Jones, P.D., Kelly, P.M., 2019. IPCC Special Report on Global Warming, Intergovernmental Panel on Climate Change. https://doi.org/10.1038/291285a0

Yang, K., Ryu, Y., Dechant, B., Berry, J.A., Hwang, Y., Jiang, C., Kang, M., Kim, J., Kimm, H., Kornfeld, A., Yang, X., 2018. Sun-induced chlorophyll fluorescence is more strongly related to absorbed light than to photosynthesis at half-hourly resolution in a rice paddy. Remote Sens. Environ. 216, 658–673. https://doi.org/10.1016/j.rse.2018.07.008

Zadeh, L.A., 1965. Fuzzy sets. Inf. Control 8, 338–353. https://doi.org/10.1016/S0019-9958(65)90241-X

CHAPTER 2

Review of Top-of-Canopy Sun-induced Fluorescence (SIF) studies from ground, UAV, airborne to spaceborne observations

Subhajit Bandopadhyay, Anshu Rastogi, and Radosław Juszczak. "Review of Top-of-Canopy Sun-Induced Fluorescence (SIF) studies from ground, UAV, airborne to spaceborne observations." *Sensors*, 2020, 20, 1144.
DOI: https://doi.org/10.3390/s20041144

Review of Top-of-Canopy Sun-Induced Fluorescence (SIF) Studies From Ground, UAV, Airborne to Spaceborne Observations

Subhajit Bandopadhyay *, Anshu Rastogi and Radosław Juszczak *

Laboratory of Bioclimatology, Department of Ecology and Environmental Protection, Faculty of Environmental Engineering and Spatial Management, Poznan University of Life Sciences, Poznan 60-649, Poland.

* Correspondence: subhajit.bandopadhyay@mail.up.poznan.pl (S.B.); radoslaw.juszczak@up.poznan.pl (R.J.)

Abstract: Remote sensing (RS) of sun-induced fluorescence (SIF) has emerged as a promising indicator of photosynthetic activity and related stress from the leaf to the ecosystem level. The implementation of modern RS technology on SIF is highly motivated by the direct link of SIF to the core of photosynthetic machinery. In the last few decades, a lot of studies have been conducted on SIF measurement techniques, retrieval algorithms, modeling, application, validation, and radiative transfer processes, incorporating different RS observations (i.e., ground, unmanned aerial vehicle (UAV), airborne, and spaceborne). These studies have made a significant contribution to the enrichment of SIF science over time. However, to realize the potential of SIF and to explore its full spectrum using different RS observations, a complete document of existing SIF studies is needed. Considering this gap, we have performed a detailed review of current SIF studies from the ground, UAV, airborne, and spaceborne observations. In this review, we have discussed the in-depth interpretation of each SIF study using four RS platforms. The limitations and challenges of SIF studies have also been discussed to motivate future research and subsequently overcome them. This detailed review of SIF studies will help, support, and inspire the researchers and application-based users to consider SIF science with confidence.

Keywords: sun-induced fluorescence; remote sensing; ground observations; UAV; airborne observations; spaceborne observations

Conclusion and Future Prospects

The science of SIF incorporating modern RS technology is a rapidly emerging front advancing the knowledge in terrestrial vegetation and the global carbon cycle. Such wide and dynamic application prospects with its emerging capabilities make SIF highly attractive for global research communities. However, quantifying and applying SIF through different RS observations is an appealing prospect, but it is also very challenging [1]. In this article, we have provided an in-depth review of existing SIF studies from the ground, UAV, airborne and spaceborne measurements. However, a rule of thumb or finest practice to address the best method, application, instrument, calibration-validation process, and modeling have not been proposed. Few challenges and future directions are indicated here to motivate future research on SIF with confidence. First, the need for the validation of SIF signals is highly required, as SIF cannot be measured independently from vegetative targets; it can only be retrieved through dedicated methods. Hence, without actual

measurements, original SIF values and the accuracy of the applied method cannot be determined. Second, it is highly necessary to understand and troubleshoot the sources of uncertainties that are associated with the SIF estimation process. The accurate estimation of SIF values in physical units and its correct interpretation is essential in application, as SIF estimations are highly affected by atmospheric (i.e., aerosols and cloud cover) factors and may depend on the instrument/system configuration and stability. Thus, the estimation of SIF should be done carefully, as such challenges need to be minimized or erased. Third, in reality, the use of a particular SIF retrieval method is restricted by the instrument or sensor availability [1]. SIF data collection through RS observations should be at very high spectral resolution, which will allow the user for subsequent resampling for multispectral or hyperspectral algorithm-based SIF estimations. Fourth, the validation of SIF values is a key concern for the leaf to ecosystem-level SIF applications. Such a requirement is highly necessary when one is working with heterogeneous ecosystems. The chances of mixing signals are more prominent in heterogeneous systems in comparison to homogeneous systems. However, validation is a real challenge for sensors and instruments with limited spatial resolutions [19]. In this scenario, new-generation efficient instruments, high-resolution UAV and airborne sensors, or satellite demonstrators (such as HyPlant for the FLEX mission) are overcoming this issue in a timely manner.

In this context, the rationale behind the FLEX mission proposal is to successfully implement a satellite mission that will provide accurate SIF retrieval at both O_2A and O_2B absorption bands. Such a mission will help to reduce the spatio-temporal uncertainties associated with SIF as well as strengthen the global vegetation and carbon estimation models.

In this review, we have discussed the in-depth interpretation of the existing SIF studies from the ground, UAV, airborne, and spaceborne observations. We have demonstrated the applied methods for SIF retrieval, instruments/sensors, target areas, and the aim of the previous studies. Over time, it has been observed that the acceptance of SIF has been increased in comparison to traditional optical RS-based vegetation monitoring approaches. The performance of a novel SIF signal (evident from publications) is a current interest for researchers in comparison to traditional vegetation indices. The vegetation indices are indicators of greenness, biomass, and water content, while SIF is directly linked to the photosynthetic mechanism. Much work has been done to show the superiority of SIF over spectral vegetation indices; for example, the SIF has been shown to be a stronger proxy of GPP than EVI [174], and it was more sensitive to drought [162] or other stress factors [75-85]. The underlying mechanism behind the observation is that the SIF contains more physiological information than the spectral vegetation indices [93]. The goal of several studies was not only to demonstrate the capability for the SIF signal, but also to showcase the development of SIF retrieval methods and its application over different targets. It has been proven that the application of SIF ranging from the monitoring of plant photosynthesis, stress detection, and plant growth monitoring has been fruitfully employed along with traditional RS-based reflectance-based methods.

There is a strong possibility for the development of SIF science, particularly in the field of ground, UAV, airborne, and spaceborne SIF studies. However, it is highly necessary to continue the future efforts toward the development of technological suits and operations to capture the reliable SIF signals in a spatio-temporal framework. Hand-held devices, mobile

field instruments for ground measurements, advanced UAV sensors, advanced and precise airborne sensors, and spaceborne sensors with high SNR and radiometric stability can make a strong contribution toward the enhancement for future SIF science [19]. The efforts toward the development of airborne demonstraters for satellite missions (HyPlant for FLEX mission, CFIS for OCO-2 mission) along with the calibration–validation through novel ground systems (such as FloX box and PICCOLO-DOPPIO) are highly necessary in future SIF science to obtain accurate, reliable, and precise SIF values from any kind of homogeneous or heterogeneous ecosystems. Apart from this, systematic and efficient technical planning for ground, UAV, airborne campaigns, and spaceborne missions should be an important consideration in future SIF measurements. As SIF is highly dynamic and very sensitive to the atmospheric influences, the effective subtraction of such external effects for accurate SIF estimation should be always a prime concern in any kind of measuring campaigns. The capabilities and efficiencies in terms of the accuracy of SIF retrieval algorithms and models must be enriched so that they can work perfectly over any kind of vegetative surfaces. To get such a robust algorithm and accurate model, continuous efforts must be performed. In this regard, it is highly relevant to test all four kinds of RS platforms measured data, to develop best SIF retrievals algorithms and models. It will help to understand the plant functionality at any spatial scale. These SIF retrieval algorithms and models must be tested over both simple (grassland) and complex (forest, peatland) ecosystems where plant structural and functional diversity is maximum. However, to achieve the high accuracy of the models with reliable SIF values, sufficient spatial and temporal resolutions, high SNR, and radiometric stability is needed for any kind of SIF measuring platforms to avoid processing errors and reduce biases in SIF estimations. In a very recent trend, the assimilation of SIF datasets obtained from all four platforms along with supporting ancillary data with machine learning and deep learning modules could enrich the future of SIF science. **Author Contributions:** S.B., A.R., and R.J. conceptualized the work. SB prepared the first draft. A.R. and R.J. edited the draft. R.J. supervised the work and arranged the required funding. All authors read and approved the final manuscript.

Acknowledgments: The close links to COST Actions OPTIMISE (ES1903) and SENSECO (CA17134) led us to the idea to write this manuscript. As we have seen, that although few review-based studies were published recently, still there was a need to provide comprehensive summary of the most important studies on SIF carried out worldwide. We want to thank the anonymous reviewers for providing valuable comments to the manuscript.

Funding: This work was funded by the National Science Centre of Poland (NCN) under the project 2016/21/B/ST10/02271 (*Sun-Induced fluorescence and photosynthesis of peatland vegetation response to stress caused by water deficits and increased temperature under conditions of climate manipulation experiment*). The publication was co-financed within the framework of the Ministry of Science and Higher Education programme as „Regional Initiative Excellence" in years 2019-2022, Project No. 005/RID/2018/19.

CHAPTER 3

HyPlant-derived sun-induced fluorescence—A new opportunity to disentangle complex vegetation signals from diverse vegetation types

Subhajit Bandopadhyay, Anshu Rastogi, Uwe Rascher, Patrick Rademske, Anke Schickling, Sergio Cogliati, Tommaso Julitta et al. "Hyplant-derived sun-induced fluorescence—A new opportunity to disentangle complex vegetation signals from diverse vegetation types." *Remote Sensing*, 2019, 11, 1691.
DOI: https://doi.org/10.3390/rs11141691

Hyplant Derived Sun-Induced Fluorescence—A New Opportunity to Disentangle Complex Vegetation Signals from Diverse Vegetation Types

Subhajit Bandopadhyay[1], Anshu Rastogi[1], Uwe Rascher[2], Patrick Rademske[2], Anke Schickling[2], Sergio Cogliati[3], Tommaso Julitta[3,7], Alasdair Mac Arthur[4], Andreas Hueni[5], Enrico Tomelleri[6], Marco Celesti[3], Andreas Burkart[7], Marcin Stróżecki[1], Karolina Sakowska[8], Maciej Gąbka[9], Stanisław Rosadziński[9], Mariusz Sojka[10], Marian-Daniel Iordache[11], Ils Reusen[11], Christiaan Van Der Tol[12], Alexander Damm[5,13], Dirk Schuettemeyer[14] and Radosław Juszczak[1,*]

[1] *Department of Meteorology, Poznań University of Life Sciences, Poznan, Poland*
[2] *Institute of Biogeosciences, IBG2, Forschungszentrum Juelich GmbH, Juelich, Germany*
[3] *Department of Earth and Environmental Sciences, University of Milano-Bicocca, Milano, Italy*
[4] *School of Geosciences, University of Edinburgh, Edinburgh, UK*
[5] *Department of Geography, University of Zurich, Winterthurerstrasse 190, 8057 Zurich, Switzerland*
[6] *Faculty of Science and Technology, Free University of Bolzano/Bozen, Italy*
[7] *JB Hyperspectral Devices, Düsseldorf, Germany*
[8] *Institute of Ecology, University of Innsbruck, Sternwartestrasse 15, 6020 Innsbruck, Austria*
[9] *Department of Hydrobiology, Faculty of Biology, Adam Mickiewicz University, Poznan, Poland*
[10] *Department of Land Improvement, Env. Development and Geodesy, Poznań University of Life Sciences, Poznan, Poland.*
[11] *Center for Remote Sensing and Earth Observation Processes (VITO-TAP), Belgium*
[12] *University of Twente, Enschede, The Netherlands*
[13] *Eawag, Swiss Federal Institute of Aquatic Science and Technology, Überlandstrasse 133, 8600 Dübendorf, Switzerland*
[14] *European Space Agency, ESTEC; Noordwijk, The Netherlands*
* Correspondence: radoslaw.juszczak@up.poznan.pl

Abstract: Hyperspectral remote sensing (RS) provides unique possibilities to monitor peatland vegetation traits and their temporal dynamics at a fine spatial scale. Peatlands provide a vital contribution to ecosystem services by their massive carbon storage and wide heterogeneity. However, monitoring, understanding and disentangling the diverse vegetation traits from heterogeneous landscape using complex RS signal is challenging due to its wide biodiversity and distinctive plant species composition. In this work, we aimed to demonstrate for the first time the large heterogeneity of peatland vegetation traits using well-established vegetation indices (VIs) and Sun-Induced Fluorescence (SIF) for describing the spatial heterogeneity of the signals which may correspond to spatial diversity of biochemical and structural traits. SIF originates from the initial reactions in photosystems and is emitted at the wavelengths in between 650-780 nm, with the first peak at around 687nm and second peak around 760nm. We used the first *HyPlant* airborne data set recorded over a heterogeneous peatland area and its surrounding ecosystems (i.e. forest, grassland) in Poland. We deployed a comparative analysis of SIF and VIs obtained from differently managed and natural vegetation ecosystems as well as from diverse small scale peatland plant communities. Furthermore, spatial relationships between SIF and VIs from large scale vegetation ecosystems to small scale peatland plant communities were examined. Apart from signal variations, we observed a positive correlation between SIF and greenness sensitive VIs, whereas a negative correlation between SIF and a VI sensitive to photosynthesis was observed for large scale vegetation ecosystems. In general, higher

values of SIF were associated with higher biomass of vascular plants (associated with higher Leaf Area Index (LAI)). SIF signals, especially SIF_{760} were strongly associated with the functional diversity of the peatland vegetation. At the peatland area, higher values of SIF_{760} were associated with plant communities of high perennials, whereas, lower values of SIF_{760} indicated peatland patches dominated by *Sphagnum*. In general, SIF_{760} reflected the productivity gradient on the fen peatland, from *Sphagnum* dominated patches with the lowest SIF and fAPAR values indicating lowest productivity to the *Carex* dominated patches with the highest SIF and fAPAR indicating highest productivity.

Keywords: HyPlant; Sun-Induced Fluorescence (SIF), peatland; spectral Vegetation Indices; NDVI; SR; EVI; PRI; fAPAR, LAI, Spectral Fitting Method; airborne campaign

2. Material and Methods

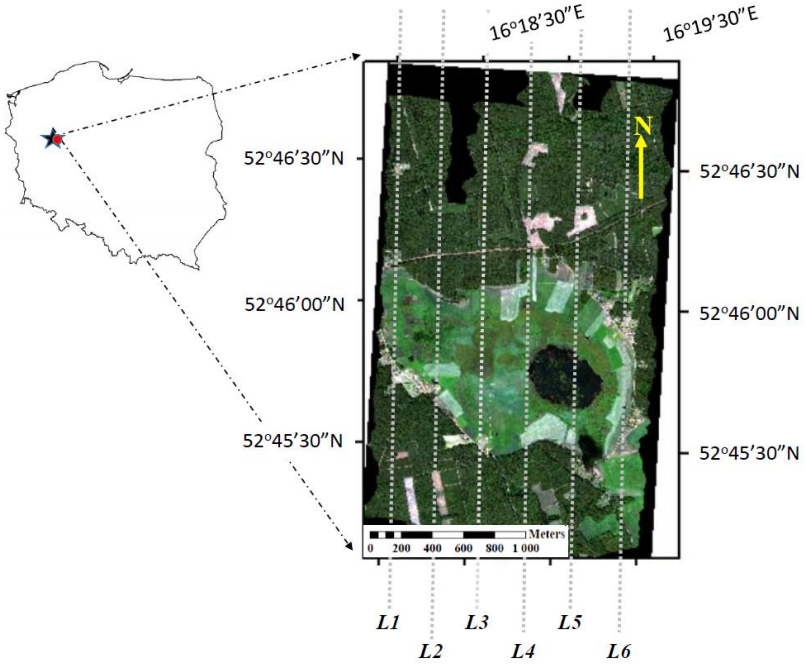

Figure 1. Location of the Rzecin peatland experimental site in Wielkopolska region, Poland. RGB composite map was obtained by combining reflectance bands at 156 nm, 105 nm, 51 nm for the red, green, and blue bands, respectively, including flight lines of the *HyPlant* over the site during the SWAMP campaign on 11th July 2015.

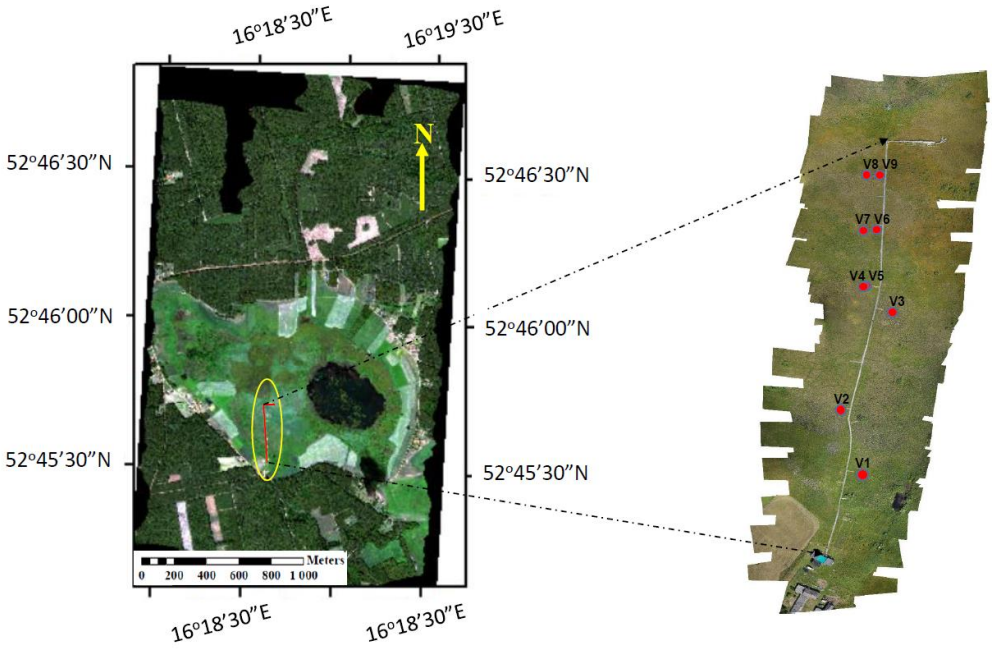

Figure 2. Location of the ground validation plots (V1-V9) at the Rzecin peatland area during the SWAMP campaign, 11th of July 2015. The plots were located on both sides of the boardwalk shown in the UAV (Unmanned Aerial Vehicle) map.

Table 2. Detailed description of the validation plots (V1 to V9) with the corresponding coordinates, dominant species, Leaf Area Index (LAI) of vascular plants and fraction of photosynthetically active radiation absorbed by plant canopy (fAPAR).

Target	Coordinates	Dominant species	LAI* ($m^2 m^{-2}$)	fAPAR* (-)
V1	52.75933°N, 16.30989°E	*Carex gracilis*	4.8±0.5	0.93±0.03
V2	52.76022°N 16.30969°E	*Carex lasiocarpa, Menyanthes trifoliata, Oxycoccus palustris, Equisetum fluviatile, Sphagnum teres*	1.7±0.5	0.68±0.19
V3	52.76067°N 16.30986°E	*Typha latifolia, Carex rostrata, Lycopus europaeus, Lythrum salicaria, Calliergonella cuspidata, Drepanocladus polycarpos, Sphagnum teres*	0.8±0.4	0.18±0.09
V4	52.76086°N 16.30975°E	*Carex rostrata, Comarum palustre, Menyanthes trifoliata, Sphagnum angustifolium, Sphagnum teres*	1.4±0.4	0.20±0.12
V5	52.76086°N 16.30975°E	*Carex rostrata, Comarum palustre, Menyanthes trifoliata, Sphagnum angustifolium, Sphagnum teres*	1.4±0.4	0.20±0.12
V6	52.76136°N 16.30969°E	*Sphagnum teres, Carex rostrata, Comarum palustre, Drosera rotundifolia*	0.9±0.3	0.12±0.07
V7	52.76136°N 16.30969°E	*Carex rostrata, Comarum palustre, Sphagnum angustifolium*	1.0±0.3	0.16±0.07
V8	52.76178°N 16.30964°E	*Sphagnum teres, Carex rostrata, Oxycoccus palustris, Drosera rotundifolia*	0.4±0.1	0.06±0.04
V9	52.76178°N 16.30964°E	*Sphagnum teres, Carex rostrate, Oxycoccus palustris, Sphagnum angustifolium,*	0.4±0.1	0.06±0.04

*LAI measured by means of SunScan system (Delta-T Devices, UK). fAPAR calculated as a ratio between APAR and incident PAR (PAR_i). APAR calculated as a difference between PAR_i and a sum of PAR transmitted trough the canopy and PAR reflected from the canopy. All PAR values measuered by SunScan system.

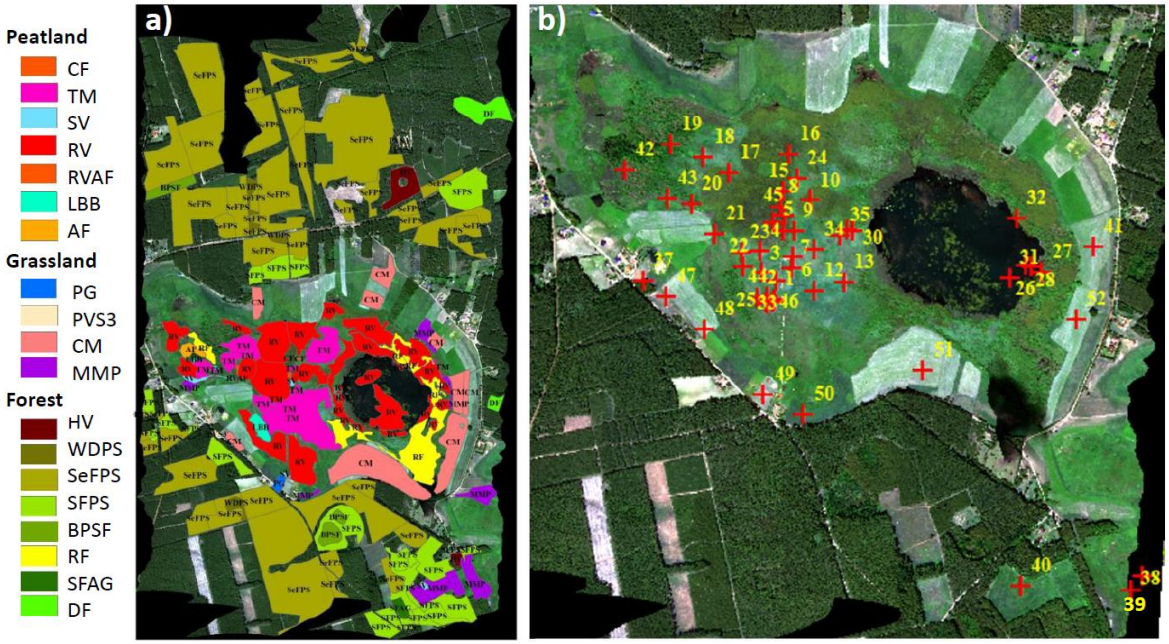

Figure 3. Boundaries of 158 ROIs identified within the *HyPlant* image and categorized into 19 unique vegetation groups (a); and location of 52 plots inside the peatland and its boundaries, categorized into 20 unique plant communities (b). Detailed characteristics of the plant communities within the 52 plots are presented in Table S1 (Supplementary Table).

Legend a): (i) **Forest vegetation groups**: herbaceous vegetation of forest clearings (HV); wooded dunes with *Pinus sylvestris* (WDPS); semi-natural forests with *Pinus sylvestris* (SeFPS); secondary forest communities with *Pinus silvestris* (SFPS); *Betula pendula* - secondary forest communities (BPFS); riparian forests (RF); secondary forest communities with *Alnus glutinosa* (SFAG); deciduous forest (DF); (ii) **Grassland vegetation groups**: post-agriculture land (PG); pioneer vegetation of sandy and shallow soils (PVS3); mowed meadows and mesic pastures (CM); meadows and mesic pastures (MMP); (iii) **Peatland vegetation groups**: calcareous fens (CF); transition mires (TM); sedge vegetation (SV); rush vegetation (RV); rush vegetation/alkaline fens (RVAF); low birch bush (LBB); alder forest (AF).

Legend b): **(i) Meadows plant communities** (ME): *Agrostis capillaris-Hieracium pilosell* (AP): 41; Mowed grassland (MG): 49,51,52; Semi mowed grassland (SMG): 48,50; *Corniculario-Corynephoretum* (CC): 37,47; *Stellario palustris-Deschampsietum caespitosae* (SPDC): 40; **(ii) Peatland Rush communities** (PR): *Cladietum marisci* (CM): 24; *Phragmitetum communis* (PC): 5,10,17,32; *Caricetum lasiocarpae* (CL): 1, 2, 11, 19, 25, 44, 46; *Thelypterido-Phragmitetum* (TP): 8; *Typhetum latifoliae* (TL): 30,43; **(iii) Fen Vegetation communities** (FE): *Caricetum diandrae* (CD): 21; *Caricetum limosae* (CLi): 14; *Caricetum paniculatae* (CP): 29,45; *Caricion lasiocarpae* (CLa): 13; Communities with dominated *Sphagnum teres* (CST): 16; *Menyantho-Sphagnetum teretis* (MST): 4; *Sphagno apiculati-Caricetum rostrata* (SACR): 3, 6, 7, 12, 15, 20, 22, 35; *Sphagno recurvi-Eriophoretum angustifolii* (SREA): 9, 18, 23, 34, 36; *Sphagno-Caricetum rostrata* (SCR): 42; *Sphagnum teres* (ST): 33.

3. Results

3.1. Interpretation of VIs and SIF for different vegetation groups

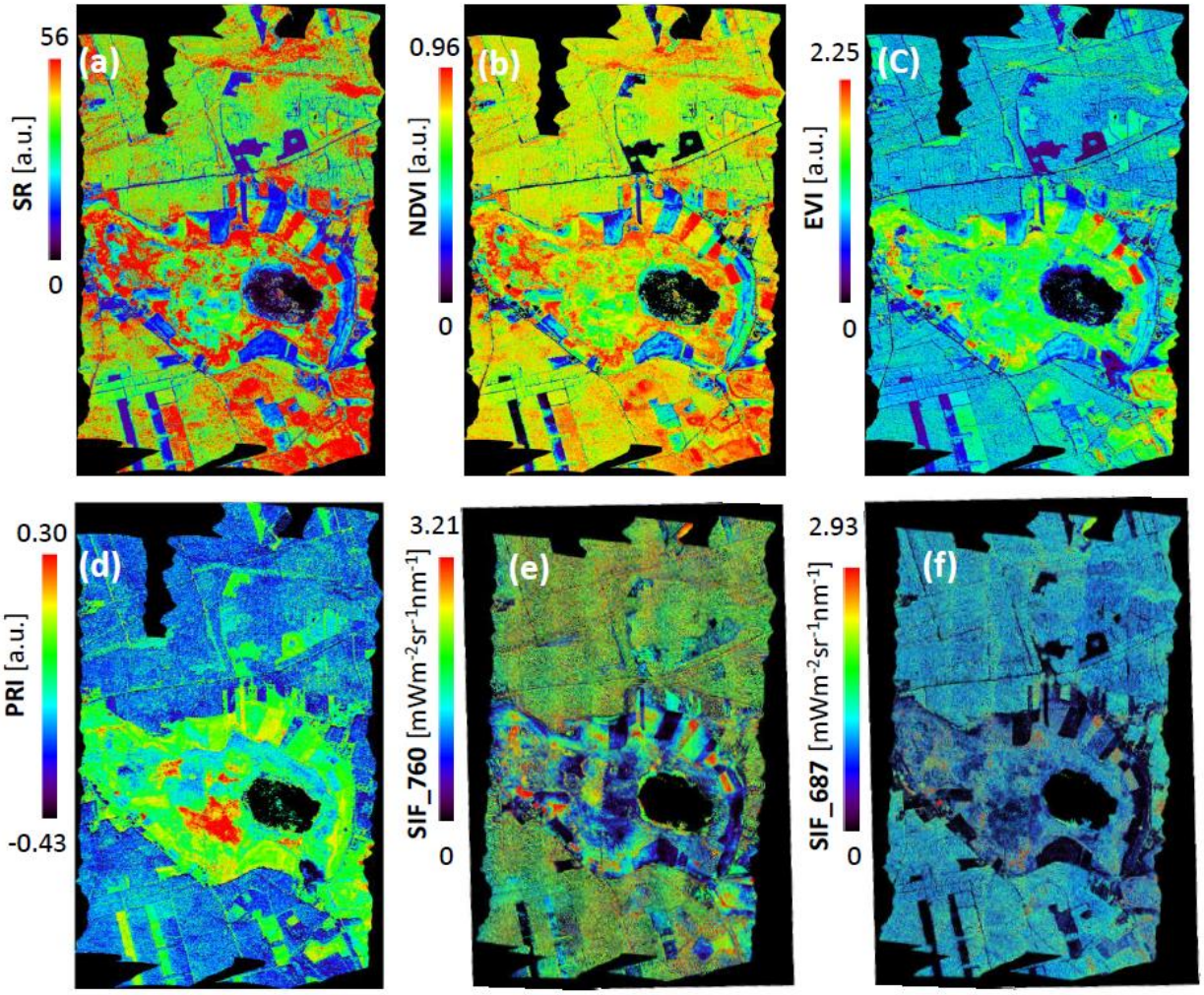

Figure 4. Airborne maps of the different vegetation indices from the experimental site derived from DUAL module (370-2500nm) of the *HyPlant* with a spatial resolution of 1m x 1m per pixel. The data was recorded on 11th July 2015 and was acquired during the afternoon overpasses of *HyPlant*. (a) Simple Ratio (SR), (b) Normalized Difference Vegetation Index (NDVI), (c) Enhanced Vegetation Index (EVI), (d) Photochemical Reflectance Index (PRI), (e) SIF map for O_2A (760 nm), and (f) SIF map for O_2B (687 nm). The associated range of each vegetation indices and SIF maps is represented in colour stretch on the left.

3.2. Validation of VIs and SIF maps from HyPlant

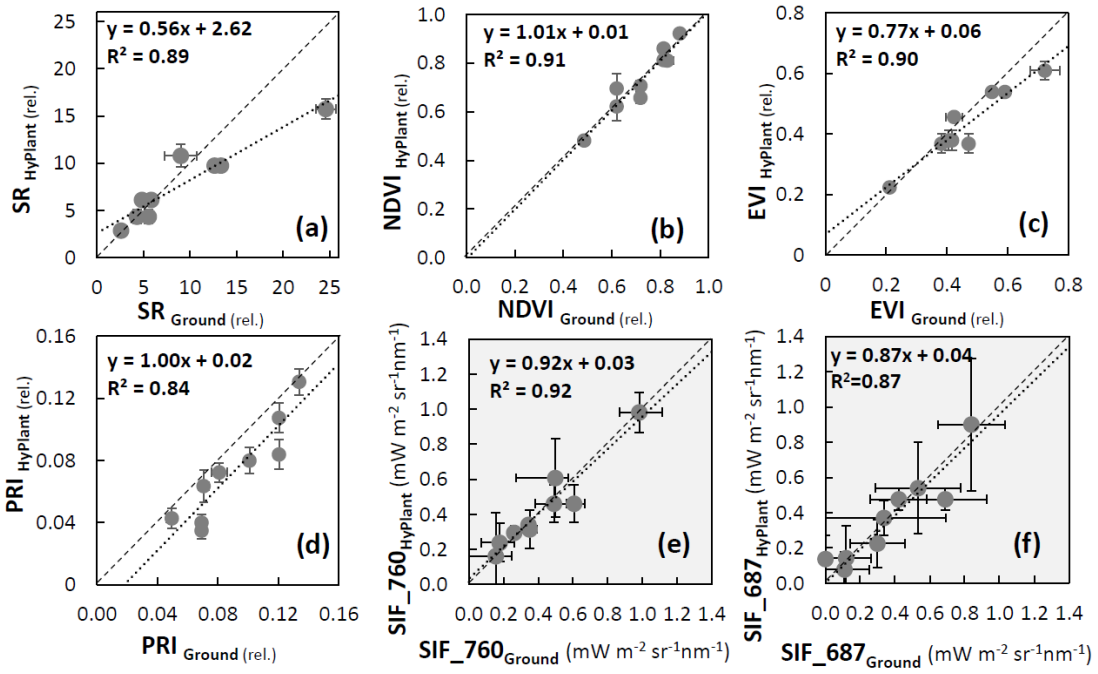

Figure 5. Validation of airborne *HyPlant* derived VIs and SIF with the ground observations on corresponding plots; (a) SR, (b) NDVI, (c) EVI, (d) PRI, (e) SIF at 760 nm (f) SIF at 687 nm. Error bars represent the spatial variability of the index values within the selected plots during *HyPlant* overpasses. Note: *HyPlant* SIF values were retrieved from the rescaled data (for details see section 2.3.1).

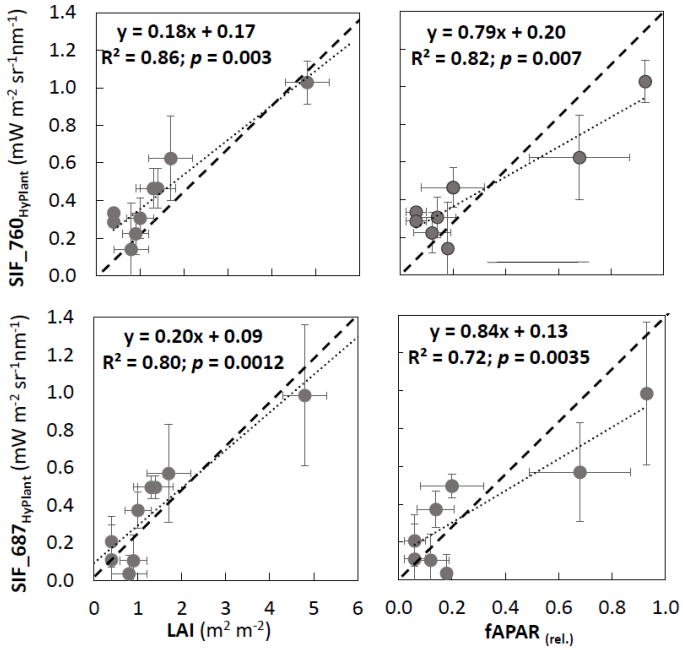

Figure 6. Relationship between *HyPlant* derived SIF and LAI and fAPAR at the ground validation plots. Note: *HyPlant* SIF values were retrieved from the rescaled data (for details see section 2.3.1).

3.3. Analysis of VIs and SIF at vegetation group level (for peatland, grassland and forest ecosystems)

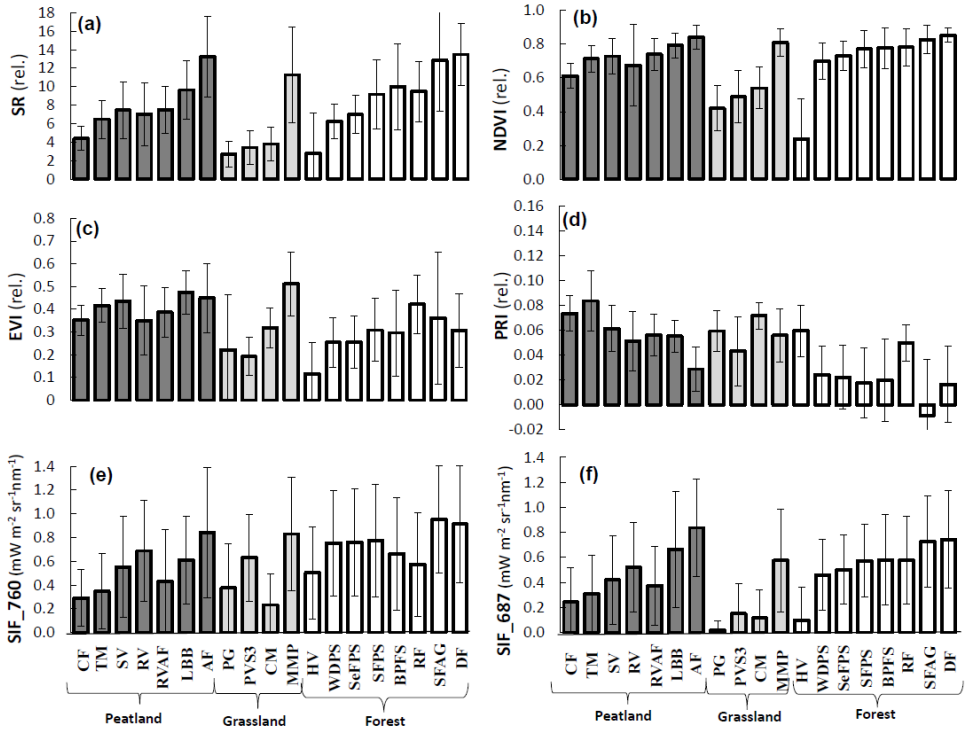

Figure 7. Bar diagram presenting the average values of the observed VIs and SIF derived from *HyPlant* data; (a) SR, (b) NDVI, (c) EVI, (d) PRI, (e) SIF_{760}, (f) SIF_{687}. The names of the individual vegetation groups are written in the bottom of the bars and correspond to the abbreviations provided with Figure 3a. Dark grey group of bars represents the peatland ecosystem; light grey bars represent different kinds of grasslands (including the post-agricultural land, pioneer vegetation of sandy and shallow soil); and white grey bars stand for different kind of forests. Error bars represent standard deviation.

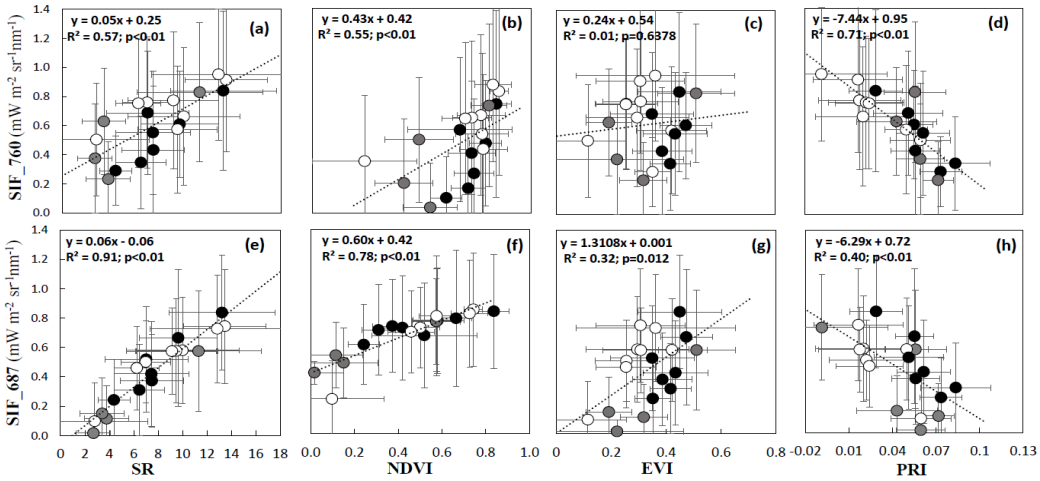

Figure 8. Correlation analysis of SIF at 760 nm (Figures a to d) and at 687 nm (Figures e to h) with selected remotely sensed VIs (SR, NDVI, and PRI) at the vegetation group level. Error bars represent standard deviation. Here, black dots denote peatland, light grey dots denotes grasslands, and white represents forest vegetation groups.

3.4. Performance of VIs and SIF signals at the peatland plant community level

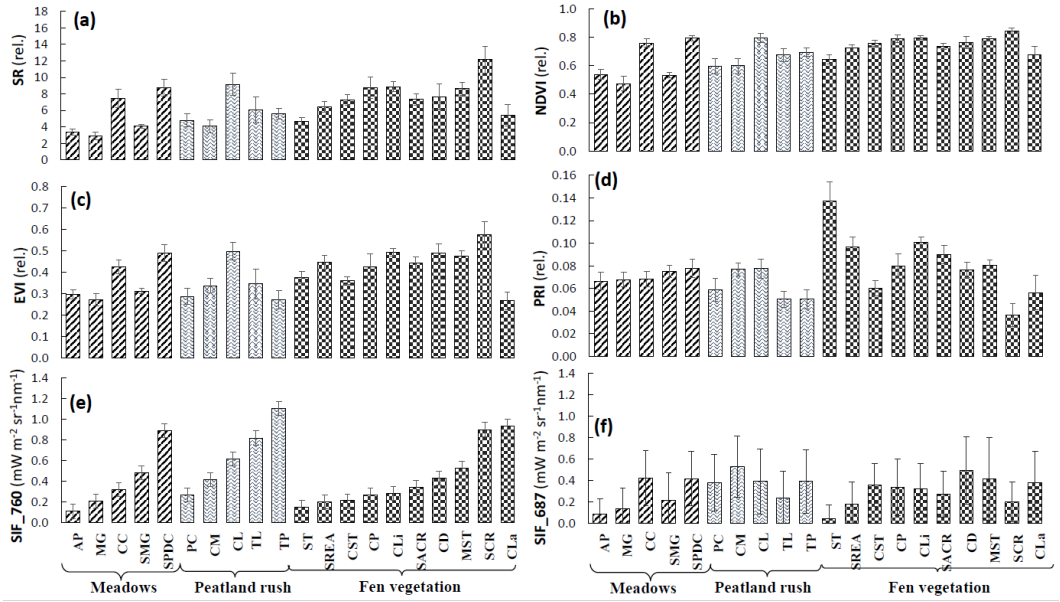

Figure 9. Bar diagram presenting the average values of the observed vegetation indices and SIF derived from *HyPlant* data; (a) SR, (b) NDVI, (c) EVI, (d) PRI, (e) SIF_{760}, and (f) SIF_{687}. The codes corresponding to the names of the individual plant communities are written at the bottom of the bars and corresponds to the abbreviations provided with Figure 3b. Detail description of these plant communities is provided in Table S1 (supplementary material). The first group of bars represents meadows (ME), the second group of bars represents peatland rush (PR) vegetation communities, and the third group of bars stands for the fen (FE) vegetation communities. Error bars represent standard deviation.

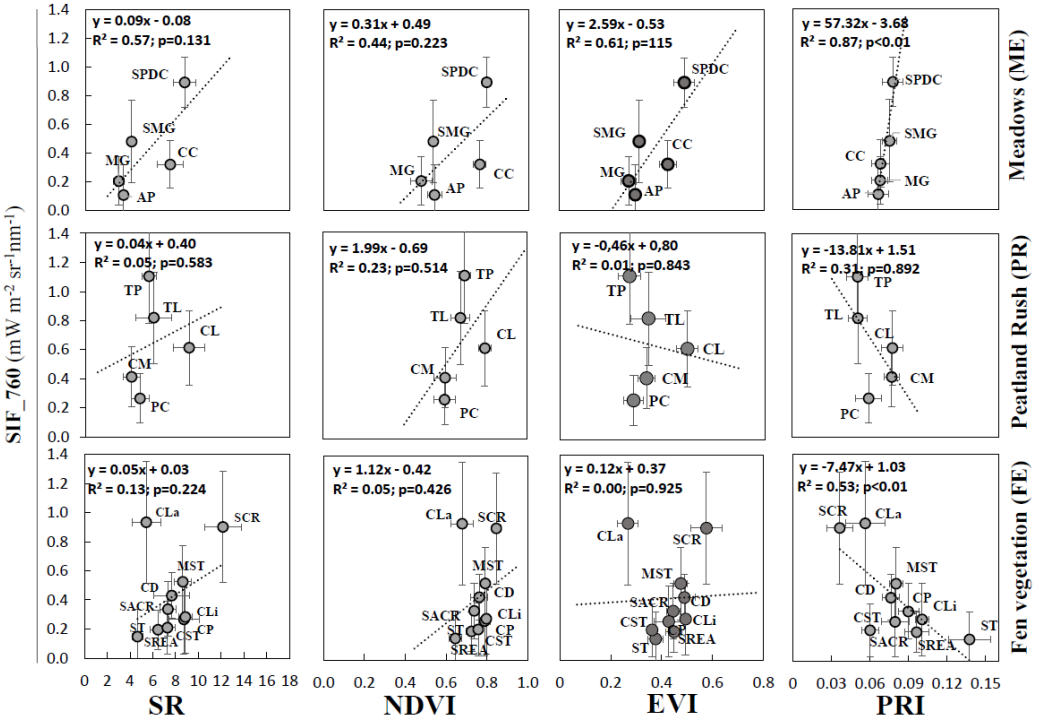

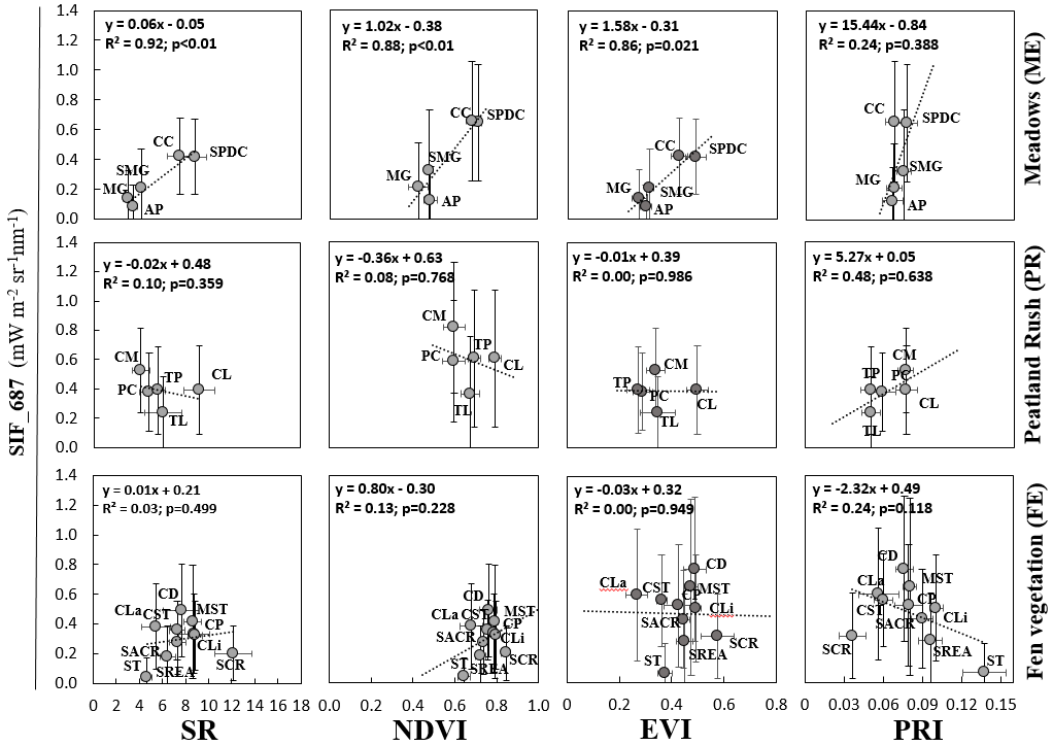

Figure 10. Correlation analysis of SIF at 760 nm and at 687 nm with selected remotely sensed vegetation indices (SR, NDVI, EVI, and PRI) at vegetation community level restricted to peatland area. Plant communities were grouped for three categories of meadows (ME), peatland rush vegetation (PR) and fen vegetation (FE), and were presented separately for each group. Codes names correspond to those provided with Figure 3. Error bars represent standard deviation.

5. Conclusions

Our results are the first experimental evidence of the possibility to retrieve both red (SIF_{687}) and far-red (SIF_{760}) chlorophyll fluorescence signals over heterogeneous ecosystems such as peatlands. The reliability and capacity of a novel airborne *HyPlant* sensor were also demonstrated in this paper that successfully captures complex vegetation signals from extremely heterogeneous peatland. The results are valid for some specific conditions and status of the peatland dependent on the hydrometeorological and climatological conditions related to the summer conditions. Hence, the findings cannot be extrapolated and may not be valid out of the season when status of the peatland, greenness of the surface, and biomass of plants are different.

Although all the results of this study depend on one-day airborne measurement, the results have illustrated a promising method to understand the dynamic degree of relationships between SIF and VIs at different hierarchical scales using *HyPlant*, the airborne demonstrator of ESA FLEX mission. We conclude on the importance of hyperspectral RS information representing a diverse set of vegetation traits including biochemical, structural, and functional traits to comprehensively assess the complex ecosystems such as peatlands and to capture the wide diversity of different vegetation groups and peatland plant communities.

In such a complex ecosystems like peatlands, we suggest quantifying and analysing red and far-red fluorescence peaks to improve our understanding and facilitate predictions

of functional dynamics in larger vegetation groups and small plant community levels, which are determined by complex interplays between functional and structural regulations.

Comprehensive measurements of SIF, fAPAR, LAI, and VIs help in the advance estimations of photosynthesis activity, biochemical and structural traits, and facilitate assessments of the wide functional diversity of vegetation groups and plant communities occurring in such ecosystems. Since SIF is considered as a prime indicator of photosynthetic activity, and is clearly correlated with fAPAR and LAI, we can assume that diversity in SIF maps reflects the diversity in their photosynthetic activity which may correspond to photosynthetising biomass of vascular plants. Our results successfully support this claim for the first time in heterogeneous surfaces like peatland. This may further enrich our knowledge in a local, regional and global understanding of the photosynthetic activity of natural ecosystems.

Acknowledgments: The Research was co-funded by the COST Action ES1309 OPTIMISE, FP7 European Facility for Airborne Research (EUFAR), FLEX-EU ESA (Contract No. 4000107143/12/NL/FF/If CCN3) and European Space Agency which supported the SWAMP training course and airborne campaigns held on 11th of July 2015. Analyses of the data and manuscript writing were carried out within the project No 2016/21/B/ST10/02271 (*Sun Induced fluorescence and photosynthesis of peatland vegetation response to stress caused by water deficits and increased temperature under conditions of climate manipulation experiment*) funded by National Science Centre of Poland (NCN).

Herby, we would like to acknowledge also contribution of students, PhD students and post-docs taking part in the SWAMP training course held in Poland in July 2015, who were involved in the SWAMP airborne campaign and took measurements of different spectral and biophysical parameters of peatland vegetation not used in this study (Violeta Andreea Anastase, Elias Fernando Berra, Conor Cahalane, Wojciech Ciężkowski, Dimitri Dauwe, Rocio Hernandez-Clemente, Fadi Kizel, Veronika Kopackova, Michał Krupiński, Titta Majasalmi, Jacques Malaprade, Antonio Padavano, Victor Rodriguez-Galiano, Magdalena Śmigaj, Dimitris Stratoulias, Joanna Suliga, Jolien Verhelst, Zhihui Wang and Youngguang Zhang). Furthermore, we would like to thank also the staff of the Meteorology Department of Poznan University of Life Sciences, who helped us in organization of the SWAMP training course and airborne campaign (Bogdan Chojnicki, Damian Józefczyk, Kamila Harenda, Klaudia Ziemblińska, Janusz Olejnik, Jerzy Roszkiewicz). Authors declare no conflict of interest.

Author Contributions: *Conceptualization*- SB; AR; UR, RJ, *Data Curation*- SB, PR, AS, SC, MG, SR, RJ, *Formal Analysis*- SB, PR, SC, MS, RJ, *Funding Acquisition*- UR, AMA, IR, DS, RJ, *Investigation*- SB, AR, UR, PR, AS, SC, TJ, AMA, AH, ET, MC, AB, MS, KS, MG, SR, MS, MDI, IR, CVDT, AD, DS, RJ, *Methodology*- SB, UR, PR, SC, RJ, *Project Administration*- UR, AS, AMA, DS, RJ, *Resources*- UR, PR, AS, SC, AMA, MJ, RJ, *Software*- PR, SC, MS, RJ, *Supervision*- AR, UR, SC, RJ, *Validation*- SB, AS, TJ, AMA, AH, ET, AB, CVDT, AD, RJ, *Visualization*- SB, PR, SC, MG, RJ, *Writing: Original Draft*- SB, AR, SC, RJ, *Writing: Review and Editing*- SB, AR, UR, SC, AH, ET, MC, MS, CVDT, AD, RJ.

CHAPTER 4

Can Vegetation Indices Serve as Proxies for Potential Sun-Induced Fluorescence (SIF)? A Fuzzy Simulation Approach on Airborne Imaging Spectroscopy Data

Subhajit Bandopadhyay, Anshu Rastogi, Sergio Cogliati, Uwe Rascher, Maciej Gąbka, and Radosław Juszczak. "Can Vegetation Indices Serve as Proxies for Potential Sun-Induced Fluorescence (SIF)? A Fuzzy Simulation Approach on Airborne Imaging Spectroscopy Data." *Remote Sensing*, 2021, 13, 2545.
DOI : https://doi.org/10.3390/rs13132545

Can Vegetation Indices serve as Proxies for Potential Sun-induced Fluorescence (SIF)? A Fuzzy Simulation Approach on Airborne Imaging Spectroscopy data

Subhajit Bandopadhyay[1,2]*, Anshu Rastogi[1,3], Sergio Cogliati[4], Uwe Rascher[5], Maciej Gąbka[6] and Radosław Juszczak[1]*

[1]*Laboratory of Bioclimatology; Department of Ecology and Environmental Protection; Faculty of Environmental Engineering and Mechanical Engineering; Poznań University of Life Sciences; 60-649 Poznań; Poland*

[2]*Remote Sensing Laboratories (RSL); Department of Geography; University of Zürich; 8057 Zürich; Switzerland*

[3]*Faculty of Geo-Information Science and Earth Observation (ITC), University of Twente, Enschede 7500 AE, the Netherlands*

[4]*Department of Earth and Environmental Sciences, University of Milano-Bicocca, 20126 Milano, Italy*

[5]*Institute of Bio- and Geosciences, IBG-2: Plant Sciences, Forschungszentrum Jülich GmbH, Leo-Brandt-Str., 52425 Jülich, Germany*

[6]*Department of Hydrobiology, Faculty of Biology, Adam Mickiewicz University in Poznań, Uniwersytetu Poznańskiego 6, 61-614 Poznań, Poland*

* Correspondence: radoslaw.juszczak@up.poznan.pl

Abstract: In this study, we are testing a proxy for red and far-red sun-induced fluorescence (SIF) using an integrated fuzzy logic modelling approach, termed as SIF_{fuzzy} and $SIF_{fuzzy-APAR}$. The SIF emitted from the core of photosynthesis aperture and observed at the top-of-canopy is regulated by three major controlling factors: (1) light interception and absorption by canopy plant cover; (2) escape fraction of SIF photons (fesc); (3) light use efficiency and non-photochemical quenching (NPQ) processes. In our study, we proposed and validated a fuzzy logic modelling approach that uses different combinations of spectral vegetation indices (SVIs) reflecting such controlling factors to approximate the potential SIF signals at 760 nm and 687 nm. The *HyPlant* derived and field validated SVIs (i.e. SR, NDVI, EVI, NDVIre, PRI) have been processed through the membership transformation in the first stage, and in the next stage the membership transformed maps have been processed through the fuzzy Gamma simulation to calculate the SIF_{fuzzy}. To test whether the inclusion of absorbed photosynthetic active radiation (APAR) increases the accuracy of the model, the SIF_{fuzzy} was multiplied by APAR ($SIF_{fuzzy-APAR}$). The agreement between modelled SIF_{fuzzy} and actual SIF airborne retrievals expressed by R^2 ranged from 0.38 to 0.69 for SIF_{760} and from 0.85 to 0.92 for SIF_{687}. Whereas, the inclusion of APAR improved the R^2 value between $SIF_{fuzzy-APAR}$ and actual SIF. This study showed for the first time that a diverse set of SVIs considered as proxies of different vegetation traits, such as biochemical, structural, and functional can be successfully combined to work as a first-order proxy of SIF. The previous studies mainly included the far-red SIF whereas, in this study, we have also focused on red SIF along with far-red SIF. The analysis carried out at 1 m spatial resolution permits to better infer SIF behaviour at ecosystem relevant scale.

Keywords: Sun-Induced Fluorescence; SIF_{fuzzy}; $SIF_{fuzzy-APAR;}$ spectral vegetation indices; HyPlant; fuzzy logic modelling

2. Material and Methods

2.5. Fuzzy logic modelling of SIF proxy from reflectance-based vegetation indices

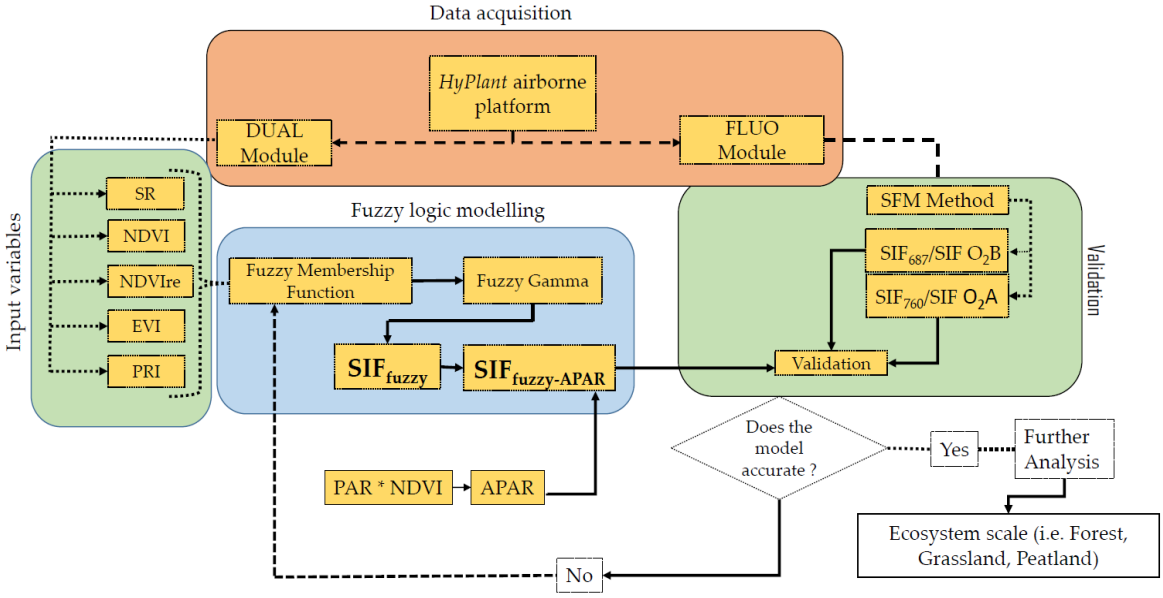

Figure 3. Scheme of the research methodology and different steps of data processing from HyPlant data acquisition to model building and validation of the outputs.

2.5.1. Fuzzy Membership Transformation

Table 2. The mathematical equations of membership functions and justifications for considering membership transformation function for individual *HyPlant* derived SVIs.

HyPlant SVIs	Membership Functions	Equations	Justifications	References
SR	Fuzzy MS Large	$\mu(x) = 1 - \frac{bs}{x - am + bs}\ if\ x > am\ otherwise\ \mu(x) = 0$	Positive strong correlation with SIF	[1]
NDVI			Positive strong correlation with SIF	[1]
NDVIre			Positive strong correlation with SIF	(Suplumetary file - Fig. S1)
EVI	Fuzzy Linear	$\mu(x) = \left\{\frac{x - min}{max - min}\right\}$	Positive poor correlation with SIF	[1]
PRI	Fuzzy MS Small	$\mu(x) = \frac{bs}{x - am + bs}\ if\ x > am\ otherwise\ \mu(x) = 1$	Negetive correlation with SIF	[1]

2.5.2. Fuzzy Overlay operation

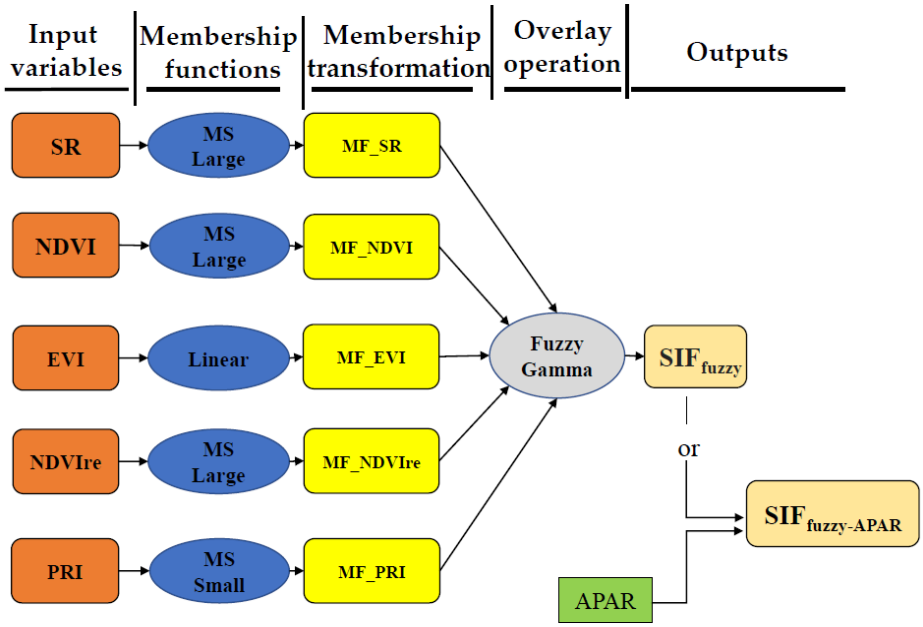

Figure 4. Schema of the fuzzy logic modelling system adopted in this study showing the progress from the input variable to the membership transformation in order to overlay operation to the final output.

2.5.3. Experiment on different fuzzy combinations

Table 3. The fuzzy logic model combinations with objectives and equations.

Combinations	Objectives	Equations	Code
Combination 1	Approximate SIF based on greenness and biomass related SVIs (without/with inclusion of APAR)	$SIF_{fuzzy} = f(NDVI + EVI)$ $SIF_{fuzzy-APAR} = f(NDVI + EVI) * APAR$	C1
Combination 2		$SIF_{fuzzy} = f(SR + EVI)$ $SIF_{fuzzy-APAR} = f(SR + EVI) * APAR$	C2
Combination 3	Approximate SIF based on greenness and xanthophyll cycle related SVIs (without/with inclusion of APAR)	$SIF_{fuzzy} = f(NDVI + PRI)$ $SIF_{fuzzy-APAR} = f(NDVI + PRI) * APAR$	C3
Combination 4		$SIF_{fuzzy} = f(SR + PRI)$ $SIF_{fuzzy-APAR} = f(SR + PRI) * APAR$	C4
Combination 5	Approximate SIF based on greenness, biomass and xanthophyll	$SIF_{fuzzy} = f(NDVI + EVI + PRI)$ $SIF_{fuzzy-APAR} = f(NDVI + EVI + PRI) * APAR$	C5

Combination 6	cycle related SVIs (without/with inclusion of APAR) Approximate SIF based on greenness, biomass, xanthophyll cycle and red-edge position related SVIs (without/with inclusion of APAR)	$SIF_{fuzzy} = f(SR + NDVI + EVI + NDVIre + PRI)$ $SIF_{fuzzy-APAR} = f(SR + NDVI + EVI + NDVIre + PRI) * APAR$	C6

*f stands for function.

3. Results

3.1. Outcome of the membership maps

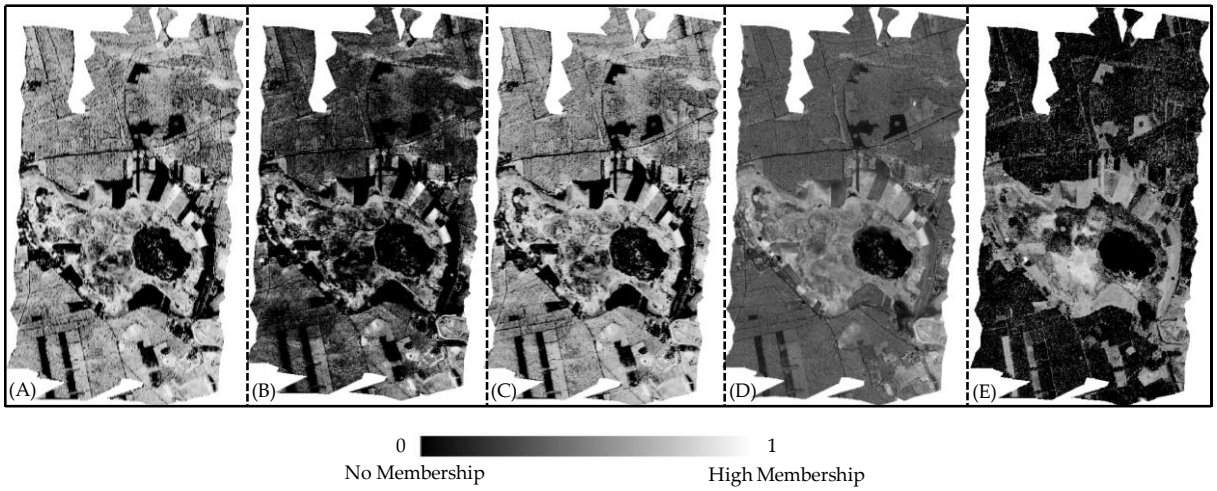

Figure 5. Membership maps of the different SVIs: A) MF_NDVI; B) MF_SR; C) MF_NDVIre; D) MF_EVI and E) MF_PRI, derived from the fuzzy membership transformation functions. The membership maps ranging from 0 to 1 represent no membership to high membership, respectively.

3.2. Performance of SIF$_{fuzzy}$

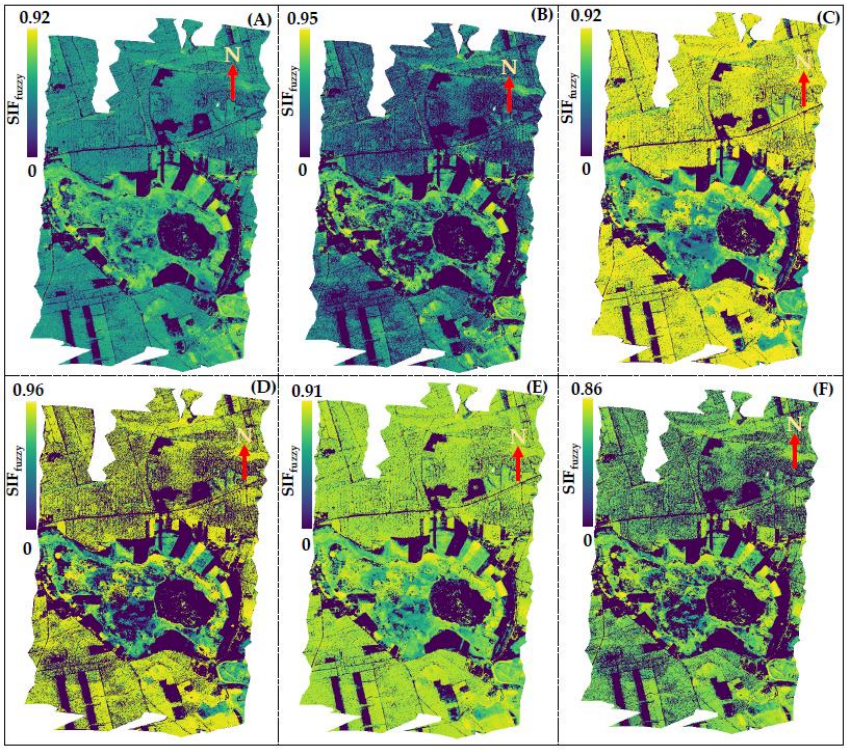

Fig. 6. Simulated SIF$_{fuzzy}$ maps developed through the integration of membership maps and fuzzy gamma approach for C1-C6 combinations: (A) C1 SIF$_{fuzzy}$; (B) C2 SIF$_{fuzzy}$; (C) C3 SIF$_{fuzzy}$; (D) C4 SIF$_{fuzzy}$; (E) C5 SIF$_{fuzzy}$; and (F) C6 SIF$_{fuzzy}$. The colour stretch in the left represents the range of C1-C6 SIF$_{fuzzy}$ maps.

Table 4. Summary of the statistics (R^2 - coefficient of determination, p-value, SE - standard error, R - correlation coefficient and RMSE - root mean square error) of linear regressions between SIF$_{fuzzy}$ vs. SIF$_{760}$ and SIF$_{fuzzy}$ vs. SIF$_{687}$. The statistical operational outputs were derived based on 19 ROIs representing vegetation groups of the forest, grassland, and peatland.

Combi-nations	SIF$_{fuzzy}$ functions	R^2	p value	SE	Pearson's r	RMSE mW·m^{-2}·sr^{-1} nm^{-1}
		SIF$_{fuzzy}$ vs. SIF$_{760}$				
C1	SIF$_{fuzzy}$ *(NDVI+EVI)*	0.38	<0.05	0.172	0.61	0.259
C2	SIF$_{fuzzy}$ *(SR+EVI)*	0.55	<0.001	0.167	0.74	0.300
C3	SIF$_{fuzzy}$ *(NDVI+PRI)*	0.61	<0.001	0.185	0.78	0.184
C4	SIF$_{fuzzy}$ *(SR+PRI)*	0.69	<0.001	0.176	0.83	0.235
C5	SIF$_{fuzzy}$ *(NDVI+EVI+PRI)*	0.51	<0.01	0.195	0.71	0.193

C6	SIF_{fuzzy} *(NDVI+EVI+NDVIre+SR+PRI)*	0.62	<0.001	0.159	0.78	0.268
	SIF_{fuzzy} vs. SIF_{687}					
C1	SIF_{fuzzy} *(NDVI+EVI)*	0.85	<0.001	0.083	0.92	0.090
C2	SIF_{fuzzy} *(SR+EVI)*	0.89	<0.001	0.083	0.94	0.114
C3	SIF_{fuzzy} *(NDVI+PRI)*	0.90	<0.001	0.092	0.95	0.154
C4	SIF_{fuzzy} *(SR+PRI)*	0.90	<0.001	0.098	0.95	0.109
C5	SIF_{fuzzy} *(NDVI+EVI+PRI)*	0.90	<0.001	0.086	0.95	0.143
C6	SIF_{fuzzy} *(NDVI+EVI+NDVIre+SR+PRI)*	0.92	<0.001	0.069	0.96	0.082

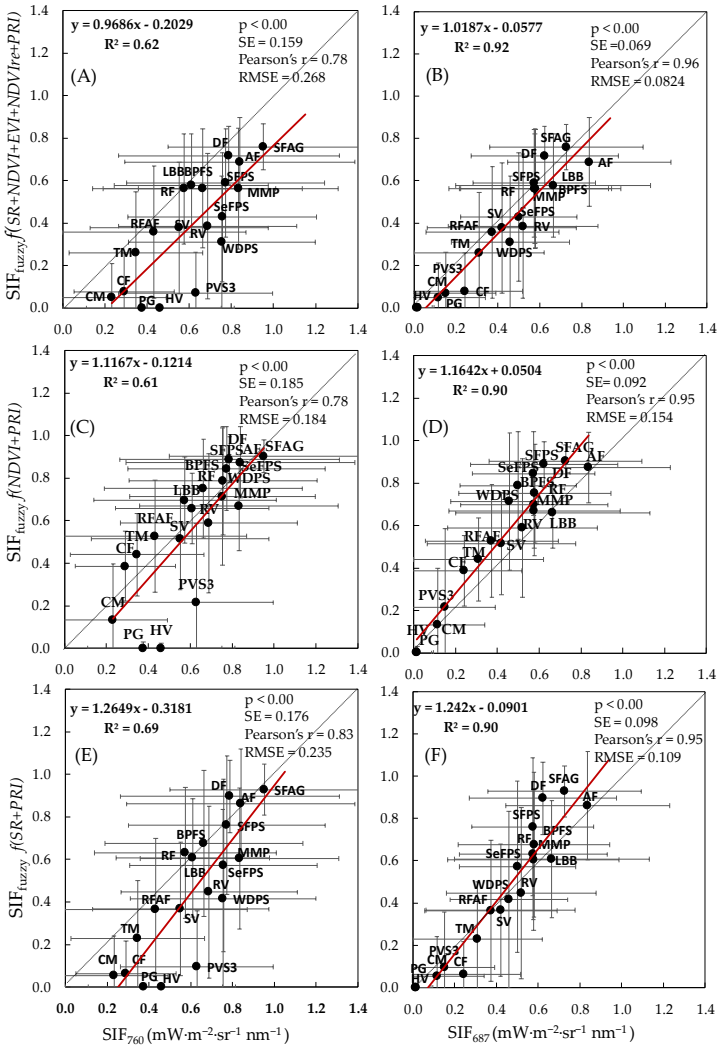

Figure 7. Scatterplots of the best performing fuzzy logic model outputs (SIF_{fuzzy}) and actual SIFs (SIF_{760} and SIF_{687}) were determined based on *HyPlant* airborne data. A & B – SIF_{fuzzy} expressed by *f(NDVI+EVI+NDVIre+SR+PRI)* under model C6; C & D - SIF_{fuzzy} expressed by *f(NDVI+PRI)* under model C3; E & F - SIF_{fuzzy} expressed by *f(SR+PRI)* under model C4. Standard deviations are represented in error bars. The letter abbreviations correspond to the codes of vegetation groups presented in Fig. 2.

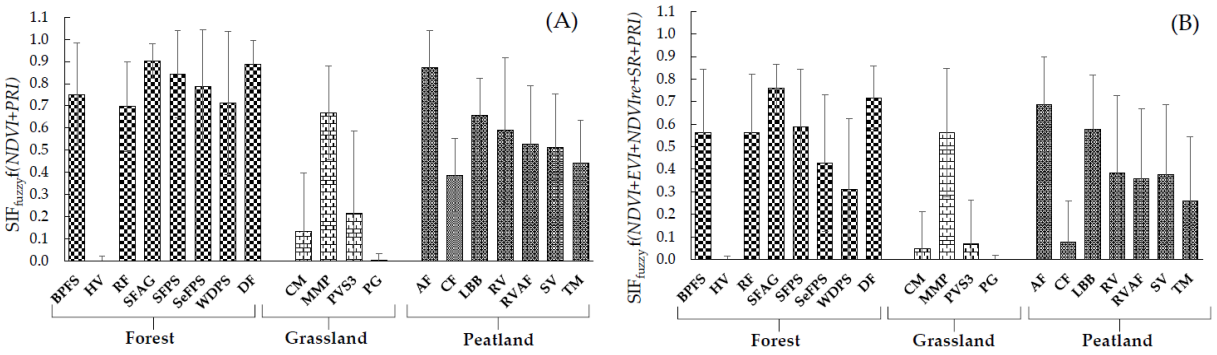

Figure 8. Example of bar diagrams represents the modelled values of SIF_{fuzzy} obtained from 19 ROIs; A) SIF_{fuzzy} as expressed by *f(NDVI+PRI)* under C3; B) SIF_{fuzzy} as expressed by *f(NDVI+EVI+NDVIre+SR+PRI)* under C6. Error bars represent the standard deviations.

5. Conclusions

The novel development of our research termed as SIF_{fuzzy} and $SIF_{fuzzy\text{-}APAR}$ was the first experimental evidence for quantitative demonstration of the fuzzy logic approach showing that the combination of SIF influencing factors represented by different SVIs can approximate the potential SIF signals at both oxygen absorption bands at 760 nm and 687 nm. It demonstrated also the efficiency of the integrated fuzzy logic model towards the step-by-step approximation of SIF signals through a process-based approach. This is also the first study that considers the red fluorescence into the prediction process which is extremely new and not covered in other published works.

Our experiment was also the first that reports the ability of simple airborne reflectance-based SVIs to produce a proxy of potential SIF. Both SIF_{fuzzy} and $SIF_{fuzzy\text{-}APAR}$ worked quite accurately to approximate the SIF signals, where SIF_{fuzzy} were closer to SIF_{687} values, whereas $SIF_{fuzzy\text{-}APAR}$ were better correlated with SIF_{760} as expressed by higher R^2 and lower RMSE.

Hence, it has been evident and recommended that the utilization of SIF_{fuzzy} under model C3 and C4 for SIF_{760} and C6 for SIF_{687} or $SIF_{fuzzy\text{-}APAR}$ under C6 for both SIF_{760} and SIF_{687} would be the optimum solution to develop the proxy of potential SIF signals at 760 nm and 687 nm with high accuracy. The study also showed that EVI and NDVI which can be available from spaceborne products can be used to approximate the SIF signals to some extent. Although this study employed one-day airborne campaign data, the outcome of this study demonstrated a promising method to develop a proxy of potential SIF, where and when SIF data is not easily available or under data constraint situations. Though the proposed method does not have a significant impact on the change of observation day, however slight changes in the agreements may occurred during seasonal changes and atmospheric anomalies.

As we have applied the HyPlant airborne datasets which is the airborne demonstrator for Fluorescence Explorer (FLEX) Sentinel 3 FLORIS satellite, we believe our study will significantly contribute to the ESA FLEX mission research and existing SIF studies. We believe also that the contribution from our study and the development of SIF_{fuzzy}, and $SIF_{fuzzy\text{-}APAR}$ models will enrich our understanding of SIF science and global carbon cycles. We have not performed the SIF_{fuzzy} and $SIF_{fuzzy\text{-}APAR}$ on the satellite dataset, but we believe that the model will work for it (however it still needed to be validated). Thus, the proposed

model is possible to be applied through satellite-derived SVIs from Sentinel 2, Landsat, MODIS, etc. to develop a SIF proxy and can be related to SIF products retrieved from spaceborne OCO-2 or GOME-2 satellites. We proved that our modelled SIF_{fuzzy} and $SIF_{fuzzy-APAR}$ are capable to reflect the diversity of potential plant photosynthetic activity from multiple ecosystems. Therefore, such studies may further develop our knowledge of the local, regional, and global photosynthetic activity and carbon cycle in natural ecosystems.

Credit authorship contribution statement: Subhajit Bandopadhyay: Conceptualization, Designing the study, Methodology, Investigation, Formal analysis, Writing – original draft and revised versions of MS, review & editing; **Anshu Rastogi:** Investigation, Methodology, Writing – revised versions of MS, review & editing; **Sergio Cogliati**: Investigation, Data Curation, Visualisation; **Uwe Rascher:** Investigation, Visualisation, Resources, Writing – revised versions of MS, review & editing, Supervision; **Maciej Gąbka**: Investigation, Formal analysis; **Radosław Juszczak**: Conceptualization, Designing the study, Methodology, Investigation, Formal analysis, Visualisation, Resources, Writing – original draft and revised versions of MS, review & editing, Supervision, Project administration, and Funding acquisition

Declaration of competing interest: The authors declare that they have no known competing financial interests or personal relationships that could have appeared to influence the work reported in this paper.

Acknowledgments: This work and analyses of the data were supported by the Polish National Research Centre (NCN) within the Project *Sun Induced fluorescence and photosynthesis of peatland vegetation response to stress caused by water deficits and increased temperature under conditions of climate manipulation experiment* (No. 2016/21/B/ST10/02271). The research was co-funded by the COST Action ES1309 OPTIMISE, FP7 European Facility for Airborne Research (EUFAR), FLEX-EU ESA (Contract No. 4000107143/12/NL/FF/If CCN3) and European Space Agency which supported the SWAMP training course and airborne campaigns held on 11th of July 2015, Poland. This work is also supported by NAWA Iwanowska Programme under the project no. PPN/IWA/2019/1/00064/U/00001. We sincerely appreciate the anonymous reviewers and members of the editorial team for their valuable comments and suggestions.

CHAPTER 5

Predicting gross primary productivity and PsnNet over a mixed ecosystem under tropical seasonal variability: a comparative study between different machine learning models and correlation-based statistical approaches

Subhajit Bandopadhyay, Lopita Pal, and Rahul Deb Das. "Predicting gross primary productivity and PsnNet over a mixed ecosystem under tropical seasonal variability: a comparative study between different machine learning models and correlation-based statistical approaches." *Journal of Applied Remote Sensing* 2021, 15(1), 014523. *DOI:* https://doi.org/10.1117/1.JRS.15.014523

Predicting GPP and PsnNet Over a Mixed Ecosystem Under Tropical Seasonal Variability: A Comparative Study between Different Machine Learning Models and Correlation-based Approaches

Subhajit Bandopadhyay[ab], Lopita Pal[c], Rahul Deb Das[d]

[a] *Laboratory of Bioclimatology, Department of Ecology and Environmental Protection, Faculty of Environmental Engineering and Spatial Management, Poznan University of Life Sciences, Poznan 60-649, Poland. Email: Subhajit.iirs@gmail.com*
[b]*Department of Geography, University of Zurich, Winterthurerstrasse 190, 8057 Zürich, Switzerland*
[c]*Department of Geography, University of Madras, India. Email: lopita1990@gmail.com*
[d]*IBM Germany Research and Development, Mies-van-der-Rohe-Straße 6, 80807 Munich, Germany. Email: das.rahuld@gmail.com*

Abstract. The global interaction of CO_2 fluxes are highly dynamic under seasonal and inter-annual variability. Thus, precise estimation of GPP and PsnNet under seasonal variations are important to understand the global carbon cycle and ecosystem response to climate variability. Considering this significance, in this paper, we have conducted a comparative investigation of correlation (i.e. Pearson product, Spearman rank, and Kendall rank) and supervised machine learning models (i.e. Random Forest- RF, Conditional Inference Forests- cForest, and Quantile Regression Forests- QRF) to explore the agreement and prediction of GPP and PsnNet under seasonal variability from spectral indices, tasseled cap transformations and reflectances over a mixed ecosystem assembling MODIS and Landsat data. Associated uncertainties and errors have been also compared. This study was carried out in a tropical moist ecosystem under pre-monsoon (March) and post-monsoon (October) conditions. Overall outcome revealed that seasonal differentiation does not affect the simple correlations, however, it has a significant impact on the GPP/PsnNet prediction process. Near-infrared (NIR) based spectral indices have been found with the best agreements and statistically significant ($p<0.001$) with GPP/PsnNet during March and October ranging coefficients from 0.85 to 0.44 in all three regression models. However, Landsat 8 OLI band reflectances in different regions of the electromagnetic spectrum have gained importance as best predictors during March, whereas NIR based indices have been found as best predictors for GPP/PsnNet during October. Anomalies in environmental and meteorological conditions have a strong impact on plant functional activities that significantly differs prediction process rather than simple correlations.

Keywords: *GPP, PsnNet, Machine Learning, Monsoon, India, Landsat*

2. Materials and Methods

2.1 Study Area

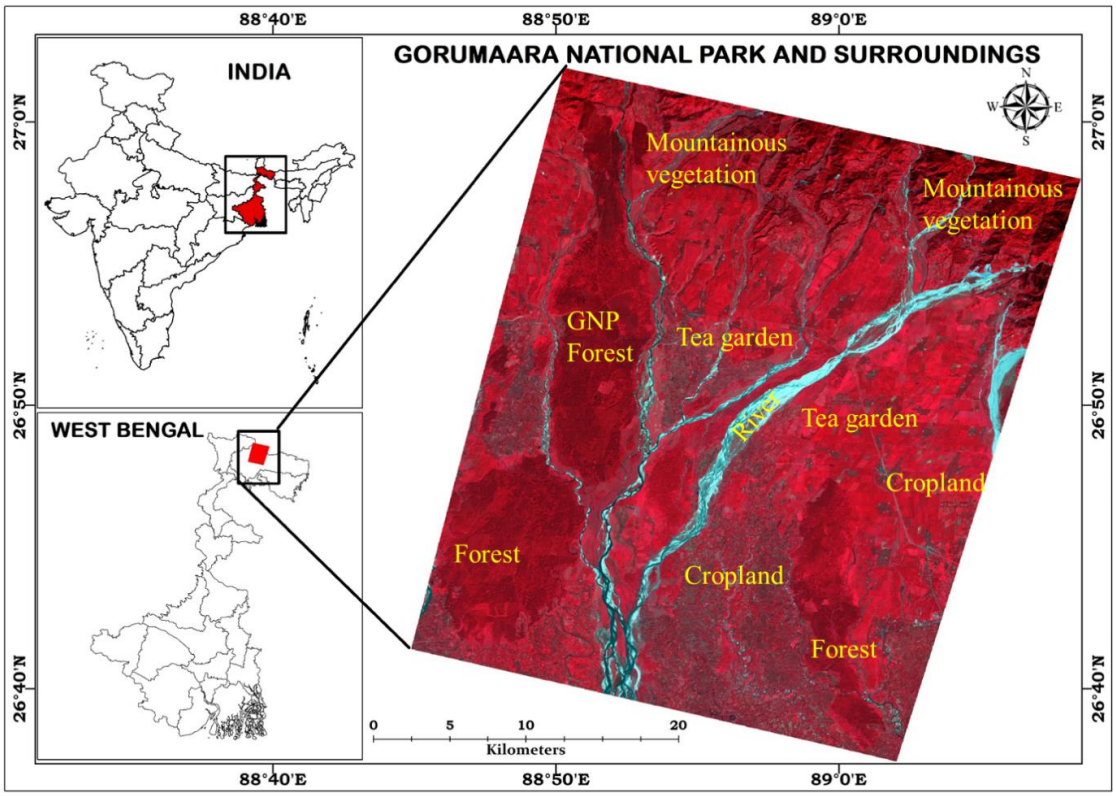

Fig. 1 Location of the Gorumara National Park (GNP) and surroundings displayed in RGB (B4, B3, B2) combination of Landsat 8 OLI. The distribution of different ecosystems was also given over the study area surveyed from high-resolution Google Earth maps.

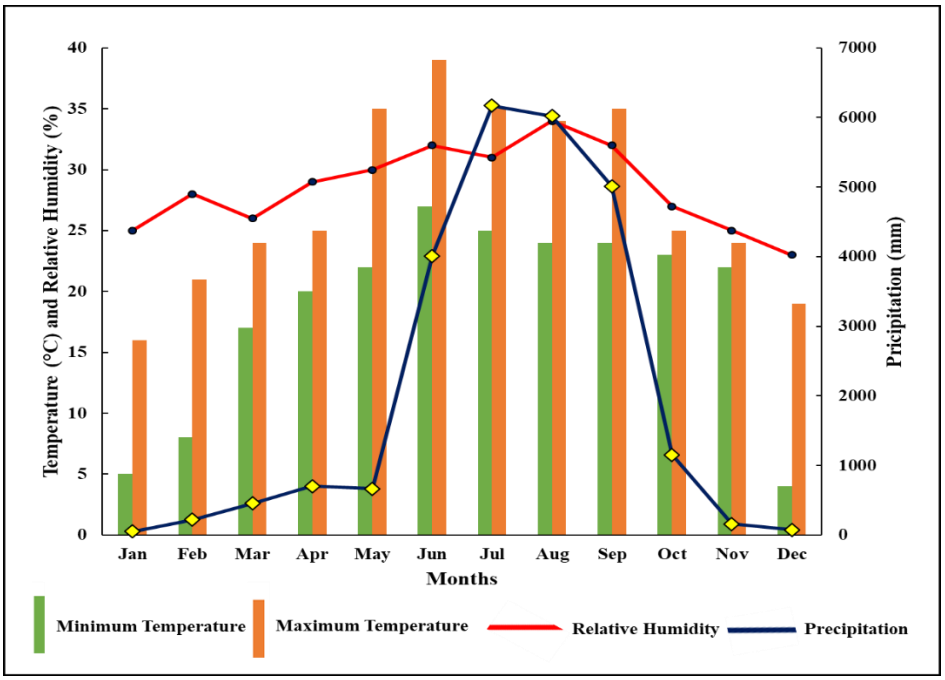

Fig. 2 The graphical representation of the climatic phenomena i.e. Temperature, Relative Humidity, Precipitation over the study area.

2.2 Datasets

Table 1 Metadata of the acquired MOD17A2H and Landsat 8 OLI data products.

	Product	Product no.	Date of acquisition	Retrieval
Pre-monsoon	MOD17A2H	MOD17A2HA2H.A2018065.h26v06.006.2018074043624	06-MAR-2018	GPP and PsnNet
	Landsat 8 OLI	LC08_L1TP_139041_20180307_20180320_01_T1	07-MAR-2018	Bands, VIs, and Tasseled Caps
Post-monsoon	MOD17A2H	MOD17A2HA2H.A2018297.h25v06.006.2018312192104	24-OCT-2018	GPP and PsnNet
	Landsat 8 OLI	LC08_L1TP_138042_20181026_20181114_01_T1	26-OCT-2018	Bands, VIs, and Tasseled Caps

2.3 Methodology

2.3.1 Downscaling of MODIS GPP and PsnNet products

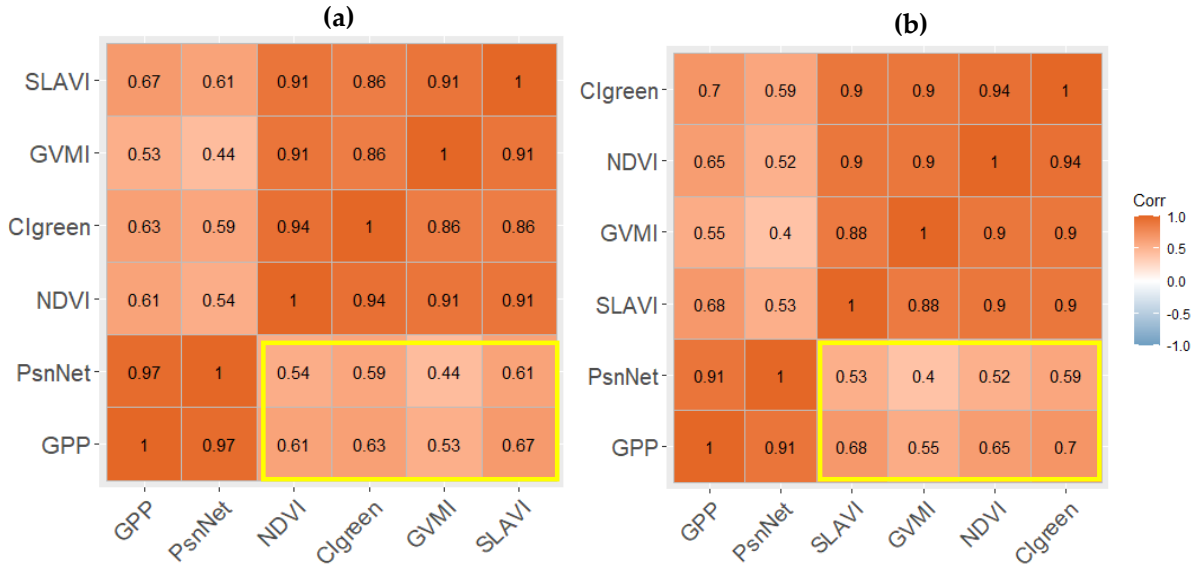

Fig. 3 Image to image correlation between downscaled MODIS 30 meter GPP/PsnNet products with Landsat 8 OLI 30 meter VIs representing different vegetation traits such as greenness content by NDVI, biomass content by SLAVI, canopy moisture content by GVMI and chlorophyll content by CIgreen (marked in yellow box). (a) Pre-Monsoon: March; (b) Post-Monsoon: October.

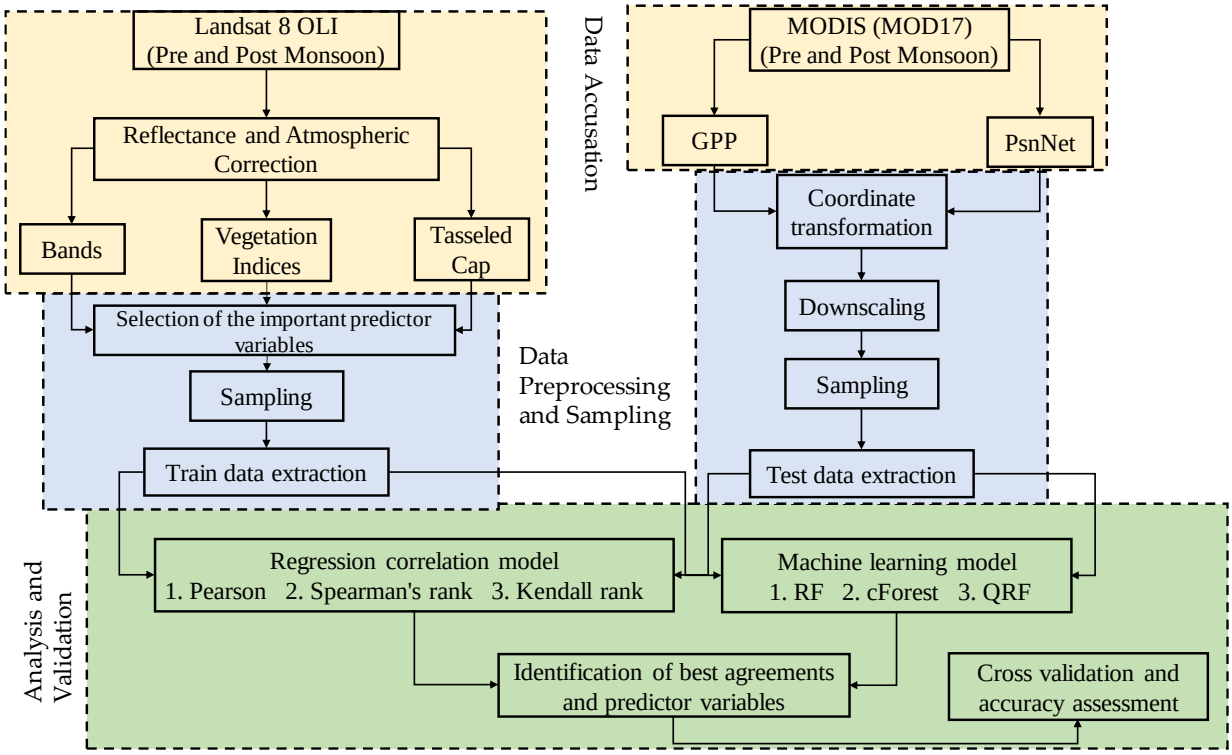

Fig. 4 Research methodology adopted for GPP and PsnNet prediction under pre and post monsoonal conditions.

3. Results

3.1 GPP and PsnNet relation under seasonal variability

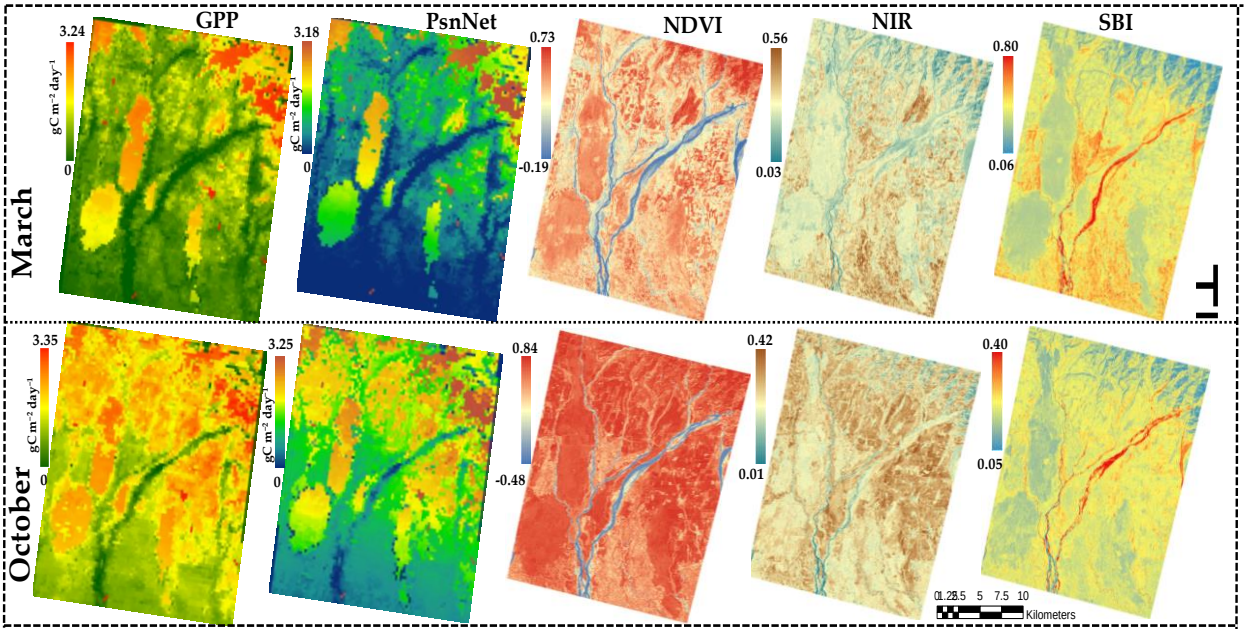

Fig. 5 Representation of GPP and PsnNet with predictor variables NDVI, NIR band and SBI during March and October 2018. One variable from each category of predictor variables (i.e. NDVI from 16 VIs, NIR from 6 L8 bands, SBI from 3 tasseled cap transformations) have been shown. Maximum and minimum of value of each image have been shown in the left. NDVI, NIR and SBI are unit less.

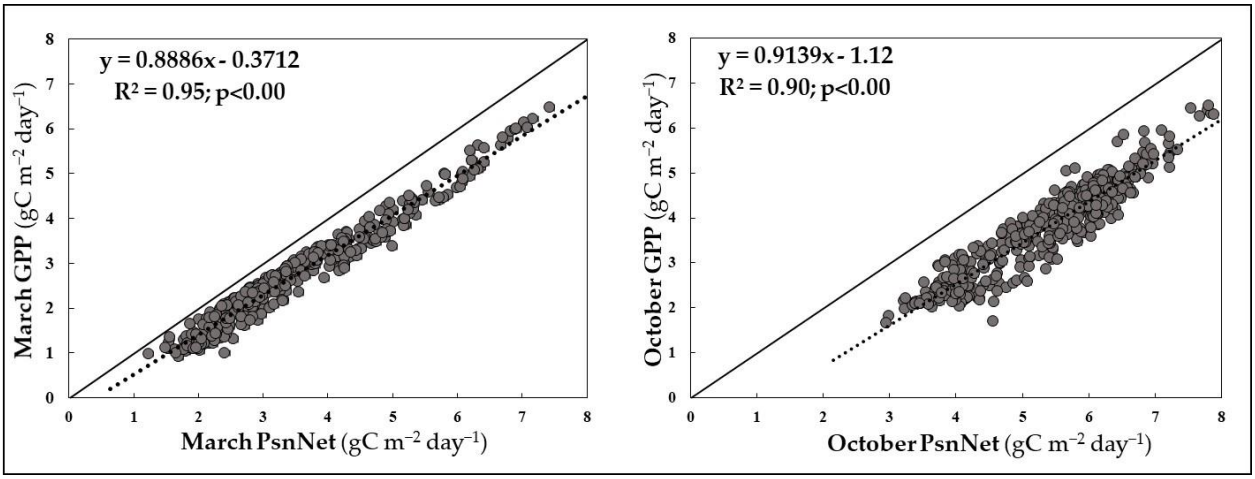

Fig. 6 Inter-relationship between GPP and PsnNet during March (pre-monsoon) and October (post-monsoon) conditions.

3.2 Selected variables from Boruta ML operation

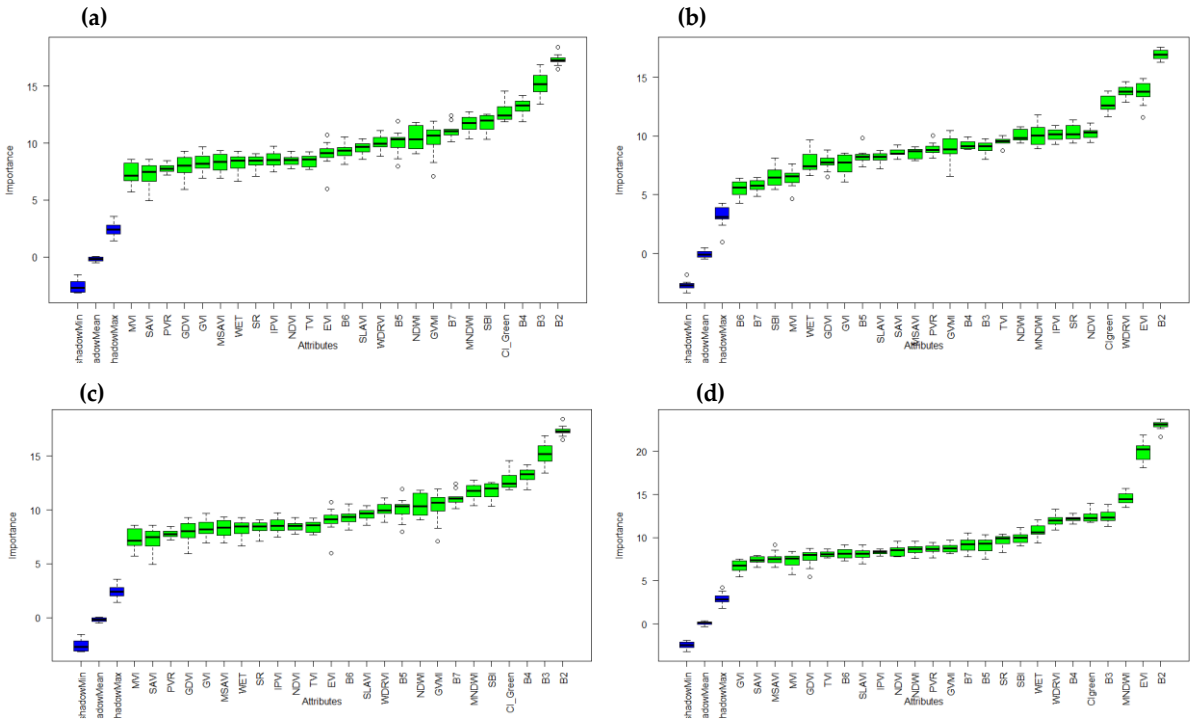

Fig. 7 Representation of feature selections using Boruta feature selection algorithm for (a) March GPP (b) October GPP and (c) March PsnNet (d) October PsnNet.

3.3 Outcome of the correlation analysis

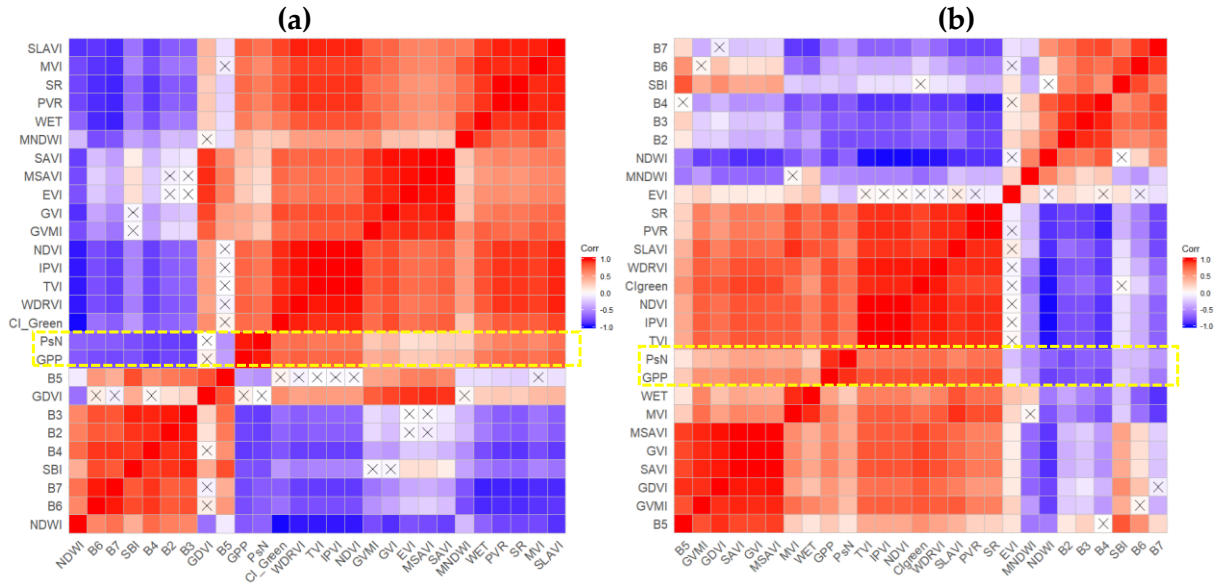

Fig. 8 The Pearson product correction between GPP and PsnNet with 25 predictor variables (6 spectral bands, 3 tasseled caps, and 16 spectral indices) during (a) March and (b) October. The red grids were showing the positive and strong agreements whereas blue grids represented the negative weak relationships. Statistically non-significant relationships were marked in cross.

3.3.2 Spearman rank correlation outcomes

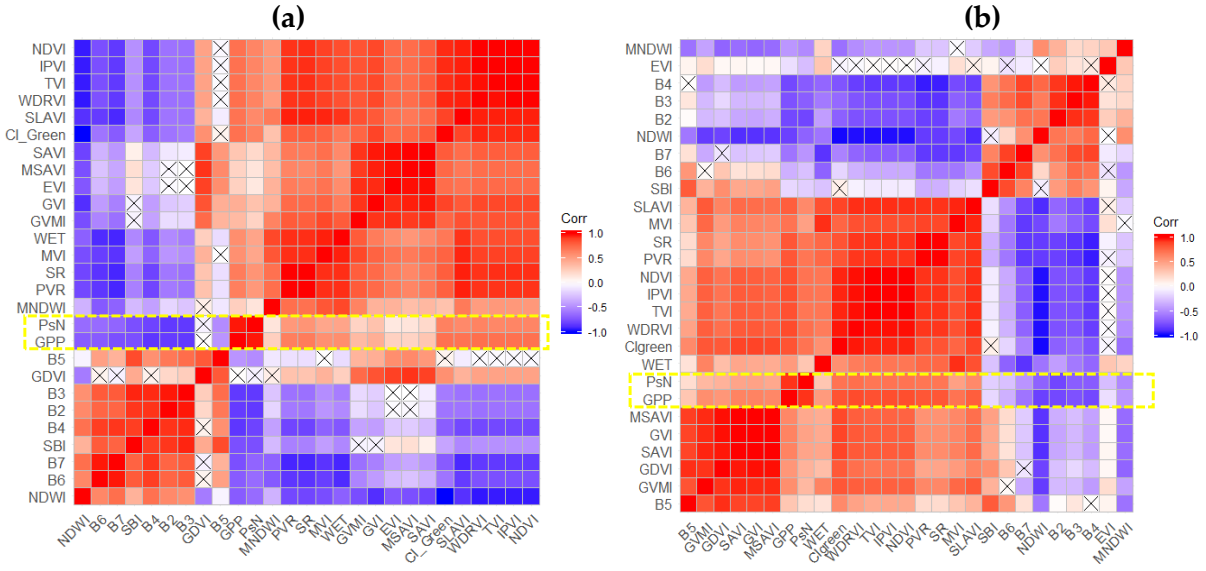

Fig. 9 The Spearman rank correction between GPP and PsnNet with 25 predictor variables (6 spectral bands, 3 tasseled caps, and 16 spectral indices) during (a) March and (b) October. The red grids were showing the positive and strong agreements whereas blue grids represented the negative weak relationships. Statistically non-significant relationships were marked in cross.

3.3.3 Kendall rank correlation outcomes

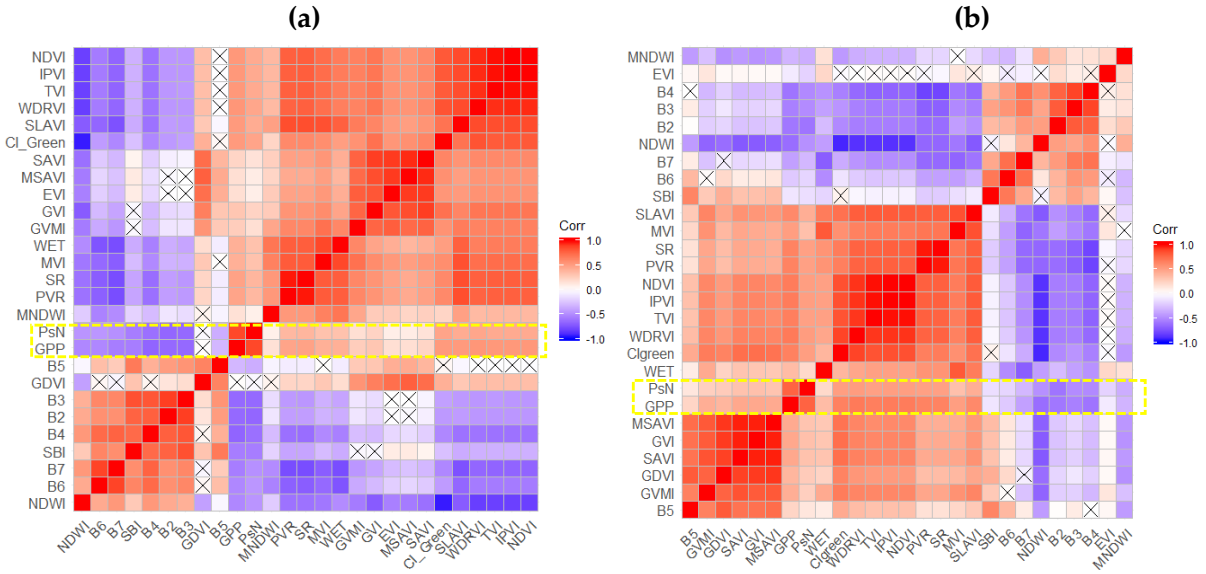

Fig. 10 The Kendall rank correction between GPP and PsnNet with 25 predictor variables (6 spectral bands, 3 tasseled caps, and 16 spectral indices) during (a) March and (b) October. The red grids were showing the positive and strong agreements whereas blue grids represented the negative weak relationships. Statistically non-significant relationships were marked in cross.

Table 3 Represents the best agreement variables for GPP and PsnNet during March and October in three correlation models namely Pearson, Spearman and Kendall rank. The degree of agreement for Pearson denoted with R, for Spearman denoted with ρ, and for Kendall rank denoted with τ. Importantly all the agreements under three models were statistically significant ($p<0.001$)

Target	Pearson Correlation (R)	Spearman Correlation (ρ)	Kendall rank correlation (τ)
March GPP	SLAVI (0.79) WDRVI (0.78) NDVI (0.75)	WDRVI (0.72) NDVI (0.71) IPVI (0.71)	WDRVI (0.53) NDVI (0.52) IPVI (0.52)
October GPP	WDRVI (0.87) SR (0.85) PVR (0.84)	WDRVI (0.85) NDVI (0.84) IPVI (0.84)	WDRVI (0.67) NDVI (0.66) IPVI (0.66)
March PsnNet	SLAVI (0.72) WDRVI (0.71) NDVI (0.70)	CIgreen (0.64) WDRVI (0.63) NDVI (0.61)	WDRVI (0.45) NDVI (0.44) IPVI (0.44)
October PsnNet	WDRVI (0.73) SR (0.72) PVR (0.71)	WDRVI (0.72) CIgreen (0.70) IPVI (0.69)	WDRVI (0.51) NDVI (0.50) IPVI (0.50)

3.4 Outcome of the predictive modelling

3.4.1 RF based prediction outcomes

Table 4: The table showed the top predictor variables, accuracy (R^2), uncertainty (RMSE), and Out-of-bag error of prediction (OOB) details of the RF based prediction model.

Target	Top predictors	R^2	RMSE (gC m^{-2} day^{-1})	OOB
March GPP	B2, B3, B4, CIgreen, B7	0.84	0.051	0.230
October GPP	B2, WDRVI, CIgreen, NDVI, WET	0.81	0.122	0.221
March PsnNet	B2, B4, B3, MNDWI, CIgreen	0.84	0.057	0.208
October PsnNet	B2, B4, WDRVI, SR, CIgreen	0.77	0.355	0.238

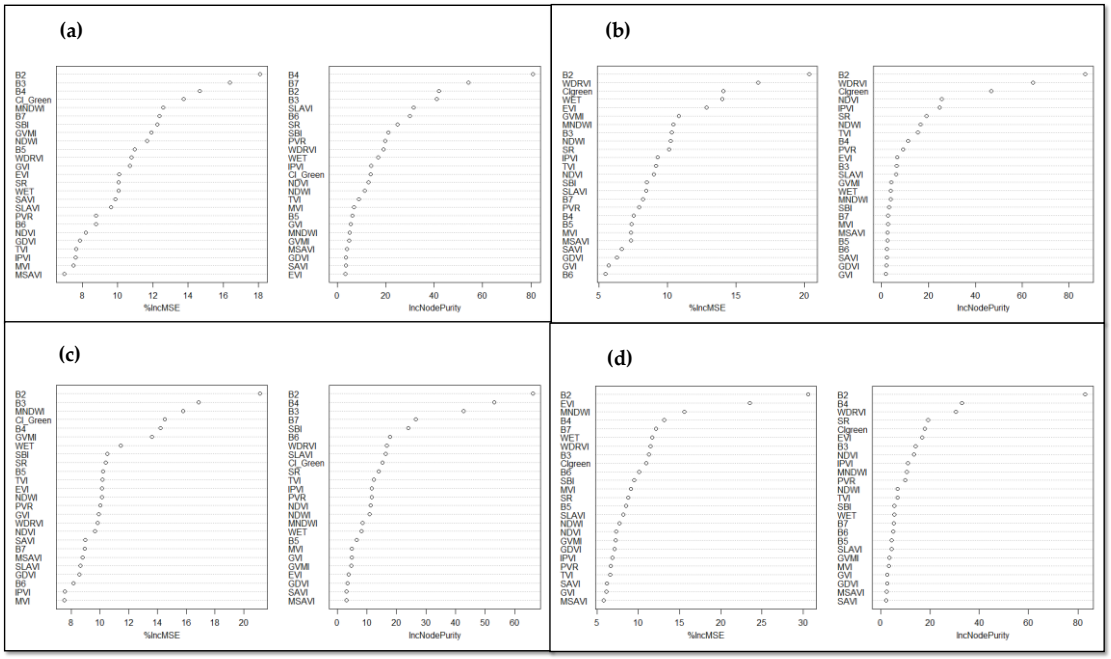

Fig. 11 Selection of optimum number of variables based on the least error for 10-fold cross-validation for the RF based prediction for GPP and PsnNet from 25 predictor variables (6 spectral bands, 3 tasseled caps, and 16 spectral indices). Fig. 10(a) March GPP, Fig. 10(b) October GPP, Fig. 10(c) March PsnNet, Fig. 10(d) October PsnNet. Variable importance reported with %IncNodePurity, and reduction in error reported in %IncMSE.

3.4.2 cForest based prediction outcomes

Table 5: The table showed the top predictor variables, accuracy (R^2), uncertainty (RMSE), and Out-of-bag error of prediction (OOB) details of the cForest based prediction model.

Target	Top predictors	R^2	RMSE (gC m^{-2} day^{-1})	OOB
March GPP	B4, B3, B2, B7, SLAVI	0.82	0.040	0.215
October GPP	WDRVI, SR, CIgreen, NDVI, IPVI	0.80	0.013	0.264
March PsnNet	B2, B3, B4, SBI, WDRVI	0.80	0.035	0.251
October PsnNet	B2, WDRVI, SR, B4, B3	0.71	0.017	0.201

3.4.3 QRF based prediction outcomes

Table 6: The table showed the top predictor variables, accuracy (R^2), uncertainty (RMSE), and Out-of-bag error of prediction (OOB) details of the QRF based prediction model.

Target	Top predictors	R^2	RMSE (gC m^{-2} day^{-1})	OOB
March GPP	B4, B7, B2, B3, SBI	0.81	0.011	0.242
October GPP	B2, WDRVI, IPVI, SR, NDVI	0.80	0.013	0.221
March PsnNet	B2, B4, B3, SBI, B7	0.81	0.042	0.218
October PsnNet	B2, EVI, MNDWI, B4, B3	0.80	0.012	0.249

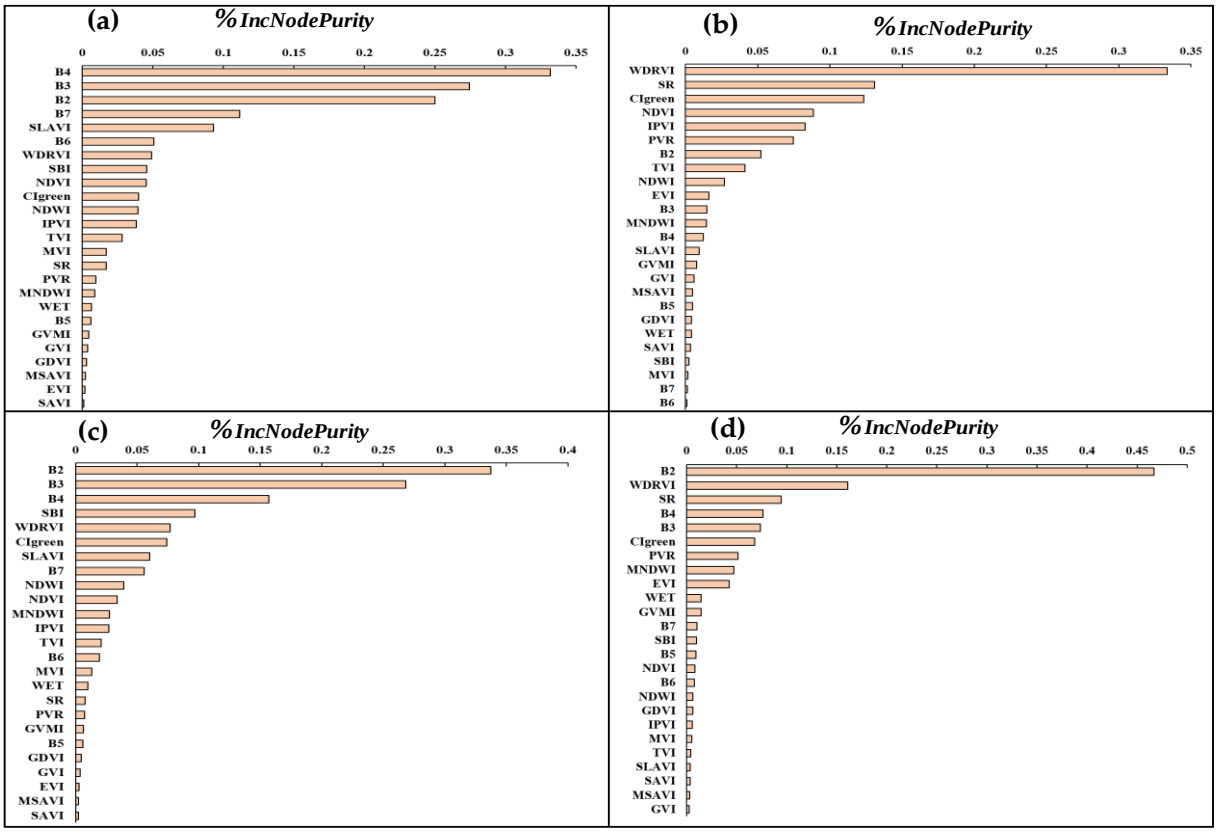

Fig. 12 Selection of optimum number of variables based on the least error for 10-fold cross-validation for the cForest based prediction for GPP and PsnNet from 25 predictor variables (6 spectral bands, 3 tasseled caps, and 16 spectral indices). Fig. 11(a) March GPP, Fig. 11(b) October GPP, Fig. 11(c) March PsnNet, Fig. 11(d) October PsnNet. Variable importance reported with %IncNodePurity.

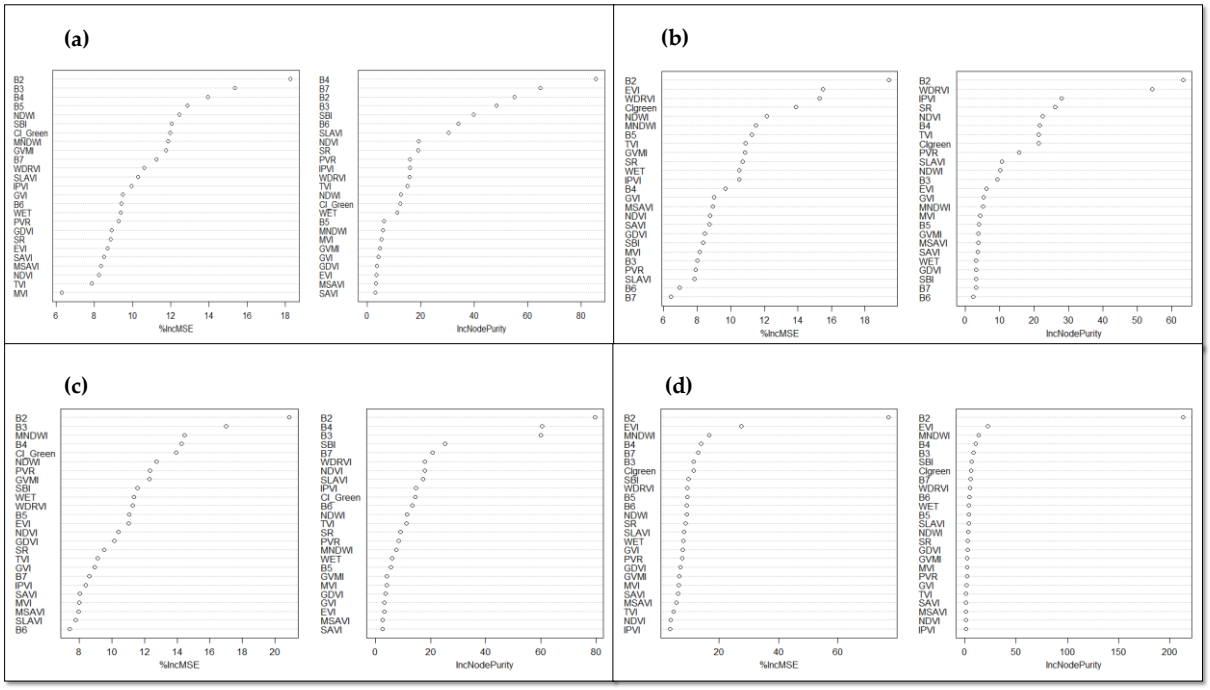

Fig. 13 Selection of optimum number of variables based on the least error for 10-fold cross-validation for the QRF based prediction for GPP and PsnNet from 25 predictor variables (6 spectral bands, 3 tasseled caps, and 16 spectral indices). Fig. 12(a) March GPP, Fig. 12(b) October GPP, Fig. 12(c) March PsnNet, Fig. 12(d) October PsnNet. Variable importance reported with %IncNodePurity and reduction in error reported in %IncMSE.

5. Conclusions

The present study highlights the utility of different reflectance regions from Landsat 8 OLI in terms of bands, spectral indices related to vegetation traits and tasseled cap transformations to predict GPP/PsnNet during seasonal and inter-annual variability. This study has also emphasized and incorporated different correlation and ML models to understand the agreement and predict the best variables for GPP/PsnNet. We have observed under changing meteorological and environmental conditions; the agreement and predictor variables are changing for GPP/PsnNet. This suggest that simple remotely sensed VIs are not sufficient to predict carbon budget in terms of GPP/PsnNet when meteorological and environmental conditions are dynamic. This study has also shown the usefulness of commonly used correlation-based techniques and current state-of-the art decision tree-based ML models for two different kind of satellite data, namely Landsat 8 and MODIS GPP products. To reduce the uncertainty in prediction process using several remotely sensed data, such approach can be used to generate the sufficiently accurate prediction models for better estimation of GPP/PsnNet, carbon budget at regional to global scale.

Four key outcomes have been derived from this study:

(1) Higher amount of net photosynthesis is proportional to higher productivity even under seasonal and inter-annual variability.

(2) Correlation-based techniques and supervised predictive models show completely different outcomes mainly during pre-monsoon March, where best predictors of GPP and PsnNet are different from the best correlation agreements with GPP and PsnNet. The best predictors and best agreement variables for GPP/PsnNet are quite similar during post-monsoon October.

(3) Environmental and meteorological differentiations during March (pre-monsoon) and October (post-monsoon) do not make any impact on the agreements between 25 predictor variables and GPP/PsnNet observed in all three correlation models.

(4) Environmental and meteorological differentiations during March (pre-monsoon) and October (post-monsoon) made an impact on GPP and PsnNet prediction process where differences can be observed among 25 predictor variables in different conditions.

Thus, it can be suggested that based on the output of the agreements, the estimation of GPP/PsnNet would be inconclusive where prediction models show different results particularly during seasonal and inter-annual variability. We believe that the comparative study that we presented in this paper, effectively identifies the uncertainties and underlying causes in GPP/PsnNet estimation process and can improve accurate estimation of carbon budget from local to global scale. Our findings will further help to gain knowledge about how the variation in climatic conditions impacts the GPP/PsnNet estimation process. This study primarily relies on MODIS GPP/PsnNet products. However future studies can explore novel Sun-induced fluorescence signal as studied by [112] for the predictive modelling of GPP/PsnNet under seasonal variability. We believe that our study will help the environmentalist, scientists, researchers, and decision makers in order to accurately estimate GPP/PsnNet. The presented work has a potential to support environmental policy makers in their decision-making process particularly in tropical ecosystems where seasonal and inter-annual diversities are quite rich.

Acknowledgements

Special thanks to the US Geological Survey, NASA, and Google earth for providing freely available satellite data. Analyses of the data were supported by the Polish National Research Centre (NCN) within the Project *Sun Induced florescence and photosynthesis of peatland vegetation response to stress caused by water deficits and increased temperature under conditions of climate manipulation experiment* (No. 2016/21/B/ST10/02271). This work is also supported by NAWA Iwanowska Programme under the project no. PPN/IWA/2019/1/00064/U/00001.
We sincerely appreciate the anonymous reviewers and members of the editorial team for their valuable comments and suggestions.

CHAPTER 6

Synthesis

Synthesis

The outcome of this thesis provides new innovative methods to explore novel SIF signals at both oxygen absorption bands over extremely complex ecosystems to enrich our deep understanding of SIF science and terrestrial photosynthetic activities. It is also the first experimental evidence of the possibility of retrieving both red (SIF_{687}) and far-red (SIF_{760}) chlorophyll fluorescence signals over heterogeneous ecosystems, such as peatlands and link these signals to different plant groups/communities. The credibility and capacity of the novel airborne HyPlant sensor which is also the airborne demonstrator of Sentinel-3 FLEX FLORIS satellite were evidenced by this thesis. Moreover, implementation of satellite derived reflectance based spectral indices, tasseled cap transformations have been utilized for GPP and PsnNet prediction process through state-of-the-art ML and corrletaion based models over a mixed ecosystem. Such research will improve our understanding on terrestrial photosynthetic activity and global carbon fluxes.

The concluding remarks of each chapter were discussed below for a better understanding of the achievements of this thesis.

The in-depth review from chapter 2 evident that the novel SIF signal incorporating modern RS technology is a rapidly emerging front in terrestrial vegetation studies and the global carbon cycle. However, the quantification and accurate estimation of SIF remain a challenge. But, the modern innovations in ground instruments, UAV sensors, frequent airborne measurements as well as ongoing and upcoming advanced satellite missions try to minimize those challenges through the innovative methods of observation. Under the conditions of modern and frequent development of sensors, instruments, retrieving algorithms, models it is difficult to address the finest practice of the best method, application, instrument, calibration-validation process, and modelling. However, the efforts toward the development of ground instruments (i.e. FloX box and PICCOLO-DOPPIO), airborne sensors (i.e. HyPlant, CFIS), and advanced spaceborne sensors (i.e. FLEX FLORIS, OCO-2, TROPOMI) have significantly improved and extended the understanding of SIF science and terrestrial vegetation activity.

Chapter 3 provides the first experimental evidence for retrieving both red (SIF_{687}) and far-red (SIF_{760}) chlorophyll fluorescence signals over heterogeneous peatland ecosystem where spectral diversity is highly rich and complex. Despite high spectral diversity, HyPlant SIF sensor successfully captured complex vegetation signals from heterogeneous surface of peatland. Though the obtained results are valid for one-day measurement, the proposed method adopted in this chapter can be illustrated for other heterogeneous landscapes. Furthermore, the adopted method to understand the dynamic relationship between SIF and VIs at different hierarchical levels can be also applied to other landscapes. In this chapter, it has been also observed that airborne obtained SIF signals can also capture the structural and functional diversity of the peatland and its surrounding ecosystems such as forest, grassland, etc. from plant community level to ecosystem scale. The simultaneous measurement of fAPAR, LAI, and VIs along with SIF signals have been also conducted at the day of airborne campaign. It helps to connect the SIF signals at both oxygen absorption

bands with vegetation biochemical, structural, and functional traits over the peatland ecosystem for the first time. The experimental evidence from this chapter provides new insights that SIF signals at both oxygen absorption bands are connected with the gradient of the plants of the peatland ecosystem and is connected to biomass of vascular plants. Though the measurement is based on one-day observation in summer, study noticed the environmental and meteorological dependency of emitting SIF signals and reflectances over the peatland vegetation. This study have also observed a connection between SIF signals and VIs that regulates the structural and functional traits of the peatland vegetation.. The key messages from this chapter will further improve our understanding of peatland, forest and grassland photosynthetic activities not only at the local scale of Rzecin peatland and its surroundings, but also in larger regional and global scales. .

Chapter 4 provides novel methodological experimental evidence to approximate the SIF signals from simple VIs using HyPlant airborne imaging spectroscopic data. The proposed SIF_{fuzzy} and $SIF_{fuzzy\text{-}APAR}$ can approximate and replicate not only the SIF_{760} but also the weaker SIF_{687} signal in an efficient way. The proposed fuzzy modelling techniques allow the step-wise approximation of the novel SIF signals and also demonstrated the capacity to approximate the red SIF signal (SIF_{687}) which is a relatively weaker signal and not much experimented with by existing literature. This work also demonstrates the first experimental evidence that reflectance-based vegetation traits can approximate and replicate the SIF_{760} and SIF_{687} signals where SIF_{fuzzy} has a higher degree of association with SIF_{687} values and $SIF_{fuzzy\text{-}APAR}$ has mainly associated with SIF_{760} values. To underastand the best combition for SIF prediction through fuzzy modelling technique, multiple combination of spectral indices in terms of their traits have been examined. Under the several combinations, this work found that SIF_{fuzzy} under the models C3 ($SIF_{fuzzy} = f$(NDVI+PRI)) and C4 ($SIF_{fuzzy} = f$(SR+PRI)) better approximate the SIF_{760} and model C6 ($SIF_{fuzzy} = f$(SR+NDVI+EVI+NDVIre+PRI)) better approximate the SIF_{687} whereas, the $SIF_{fuzzy\text{-}APAR}$ under C6 for both SIF_{760} and SIF_{687} would be the optimum solution to approximate the original SIF signals. The proposed method of fuzzy simulation can be also implemented in other study sites apart from the peatland ecosystem and also on a global scale. The evident method of fuzzy simulation can act as significant support and help to develop the proxy or replication of SIF signals from simple spaceborne or airborne SVIs under the data constraint situation as well as where SIF data is not so easily available. Though in this study fuzzy simulation has been applied over HyPlant derived SVIs, the methodology can be applied for spaceborne SVIs like EVI, NDVI derived from mostly used satellite datasets like Landsat 8, Sentinel-2, MODIS, etc. The potential SIF_{fuzzy} and $SIF_{fuzzy\text{-}APAR}$ can also represent the structural and functional diversity of the peatland ecosystem as well as for surrounding ecosystems in agreement with the Bandopadhyay et al., 2019. This may further improve our understanding of local, regional, and global photosynthetic activity and the carbon cycle. As in this work HyPlant airborne datasets have been used, it demonstrated the capabilities of the HyPlant sensor for FLEX FLORIS satellite to monitor potential SIF dynamics over multiple ecosystems.

Chapter 5 emphasized and compared different correlation methods (i.e. Pearson, Spearman rank, Kendall rank) and different ML models (RF, cForest, QRF) to explore the agreement and contribution of variables like bands, spectral indices, and tasselled cap transformations to predict the GPP and PsnNet under seasonal and inter-annual variability. This work has been found that the best agreements differed from the best predictor in relation to GPP and PsnNet in different seasonal conditions. Furthermore, this work has also found that a higher amount of PsnNet is incorporated with high productivity under both seasonal conditions. It has been observed that the environmental and meteorological conditions during March (pre-monsoon) and October (post-monsoon) have no visible impact in all three correlation models whereas the monthly variability has a strong impact on the prediction process. It has been also detected that NIR-based spectral indices like (i.e., NDVI, IPVI, SLAVI, WDRVI, and CIgreen) have strong agreement with GPP and PsnNet under both seasonal conditions. The connection between NIR and plant productivity has been well evident by this study where higher productivity, as well as higher NIR reflectance, were observed during October and vice-versa conditions in March. As the best agreements differed from the best predictors for GPP and PsnNet, therefore, it can be stated that the variables of simple correlation-based outputs were not properly represented the predictors and they are not sufficient enough to predict the GPP and PsnNet. The underlying causes and uncertainties related to in GPP and PsnNet estimation process have been also discussed in this work. The research presented in chapter 5 may improve the accurate estimation of the carbon budget from local to global scales and further it enriches our understanding of terrestrial productivity. As this study also incorporates the seasonal influences on the prediction process, it evident that climate, weather and surrounding environmental conditions have a major impact not only on vegetation productivity but also on its prediction process. This will help to enrich our existing understanding on the influences of environmental and climatic factors in terrestrial productivity under seasonal dynamics.

This work may also help the environmentalist, scientists, researchers, farmers, and decision-makers in building sustainable environmental policies under climate change conditions.